

# Cosmic Dipoles from Large-Scale Structure Surveys

Jaiyul Yoo,<sup>1,2,\*</sup> Matteo Magi,<sup>1,†</sup> and Dragan Huterer<sup>3,‡</sup>

<sup>1</sup>*Center for Theoretical Astrophysics and Cosmology, Department of Astrophysics,  
University of Zürich, Winterthurerstrasse 190, CH-8057, Zürich, Switzerland*

<sup>2</sup>*Department of Physics, University of Zürich, Winterthurerstrasse 190, CH-8057, Zürich, Switzerland*

<sup>3</sup>*Department of Physics and Leinweber Institute for Theoretical Physics,  
University of Michigan, 450 Church St, Ann Arbor, MI 48109, USA*

(Dated: December 8, 2025)

Large-scale structure surveys can be used to measure the dipole in the cosmic microwave background (CMB), in the luminosity distances inferred from type-Ia supernova observations, and in the spatial distribution of galaxies and quasars. The measurements of these cosmic dipoles appear to be mutually inconsistent, even though they are expected to indicate the common observer velocity. This observational tension may represent a significant challenge to the standard model of cosmology. Here we study in detail what contributes to the cosmic dipoles from CMB, supernova, and galaxy survey in the standard  $\Lambda$ CDM model, though our theoretical model can be applied beyond the standard model. While measurements of the cosmic dipoles yield the relative velocities between the source samples and the observer velocity, the motion of the observer is the dominant contribution in the conformal Newtonian gauge, and the intrinsic velocities of the samples fall steeply with increasing redshift of the sources. Hence the cosmic dipoles of CMB, type-Ia supernovae, and galaxies should be aligned but can have different amplitudes. We also clarify several misconceptions that are commonly found in the literature.

## I. INTRODUCTION

Large-scale structure in the Universe can be probed by tracers such as galaxies, quasars, type-Ia supernovae (SNIa), and cosmic microwave background (CMB) temperature anisotropies, and these large-scale structure tracers form an effective fluid that is described in terms of its density, velocity, and pressure. The evolution of such cosmic fluids is governed by gravity, and the current standard model in cosmology is the  $\Lambda$ CDM model with Einstein's theory of general relativity. Hence, a test of the standard model in cosmology by using the mutual relation and time evolution of the cosmic fluids is one of the ultimate goals in large-scale structure surveys. While the first moment (or the density fluctuations) and its two-point correlation function (or the power spectrum) have received most attention in large-scale structure surveys (see, e.g., [1–3]), the second moment (or peculiar velocities) and its spatial correlations also contain crucial cosmological information such as the logarithmic growth rate derivable from the redshift-space distortion [4].

In particular, the peculiar velocities of the tracers of large-scale structure measured at the position of the observer leave unique dipolar patterns, and their dipole measurements can be used to test the standard model of cosmology [5]. The observed CMB sky is nearly isotropic, with anisotropies only at the level of  $10^{-5}$ , but this isotropic sky temperature map is obtained only after subtracting the dipole pattern with an amplitude 100 times larger than the rms fluctuation amplitude. This dipole moment was measured in various CMB satellite missions [6–9], culminating with the sub-percent level measurement precision in the Planck survey [9]. Large-scale galaxy surveys also produce sky maps of galaxies, quasars, or any

other cosmological tracers (collectively referred to as galaxies) primarily as a function of angular position, with additional information of flux, redshift, and so on (see, e.g., [10, 11]). In the same way as in the CMB sky map, the peculiar velocities of these galaxy samples imprint the dipolar patterns in the galaxy sky maps, and the dipole moments can be measured for individual galaxy samples in large-scale galaxy surveys. In practice, however, it is more difficult to measure the dipole moments in galaxy surveys due to the limited sky coverage than in CMB surveys with an almost full-sky coverage. The dipole moment of a galaxy survey was first measured [12–17] in the NRAO VLA Sky Survey (NVSS; [18]). Other large-scale galaxy surveys in the following years were used to measure the dipole moments of various cosmological sources [14, 19–23] with increasing measurement precision.

The dipole patterns in the large-scale structure surveys mainly arise from the peculiar motion of the observer, and hence the direction and the amplitude of the peculiar motion in responsible for the dipole measurements should be identical to those found in the CMB sky map. This cosmological test using the dipole measurements from various large-scale structure surveys is known as the Ellis-Baldwin test [5]. From the inception of the Ellis-Baldwin test, large-scale galaxy surveys tend to report that the dipole direction is largely aligned with the CMB dipole direction, but the inferred amplitude is larger by a factor of few than in the CMB sky map (see [24] for a recent review). Such discrepancy has worsened in the recent years, and in particular the precision measurement of the dipole moment for the quasar sample from the WISE survey [25] puts the discrepancy at the  $5\text{-}\sigma$  level [21], calling for close investigations of the standard model of cosmology [26].

Here we discuss in detail what contributes to the dipole moments in large-scale structure surveys, and we clarify several misconception in the literature. For numerical computation, we adopt the standard  $\Lambda$ CDM model with cosmological parameters obtained in the Planck cosmological parameter analysis [9] and use the Boltzmann solvers (CAMB [27] and

\* jaiyul.yoo@uzh.ch

† matteo.magi@uzh.ch

‡ huterer@umich.edu

CLASS [28]) to compute our theoretical predictions. Though our analytical and numerical calculations are based on the standard cosmological model, they can be readily applied to the beyond-the-standard models. In Section II we discuss subtleties associated with relative motion and the Ellis-Baldwin test. Then in Sections III–V, we discuss the dipole moments from the CMB temperature anisotropies (§ III), the supernova surveys (§ IV), and the galaxy surveys (§ V). We discuss our findings in Section VI. The details of our calculations can be found in Appendices.

## II. SUBTLETIES IN COSMIC DIPOLES

In a homogeneous and isotropic universe (or a background universe), all observers on a time-like geodesics or observers following any fluids such as the matter and the photon fluids are at rest, and this rest frame is shared by all the observers (hence the *cosmic rest frame*). A coordinate system that describes the homogeneous and isotropic universe is uniquely determined up to the rotation and translation of the space. In a real universe with inhomogeneities, however, there is no unique way to fit a background homogeneous and isotropic universe (or a coordinate system) to the real universe. This fitting process amounts to a gauge choice [29, 30], and all gauge choices are on the same footing in general relativity with diffeomorphism symmetry. One can therefore choose *any* coordinate system (which represents a background homogeneous and isotropic universe) and work with perturbations (or the difference between the real universe and the chosen background universe at a given spacetime position). These perturbations are hence gauge-dependent (or coordinate dependent), and their interpretations also depend on the choice of gauge (see, e.g., [31–33]).

Cosmic dipoles have been measured in the past by using the CMB temperature anisotropies [6–9] and other large-scale structure probes such as supernovae [34], quasars [21], and galaxies [14, 19, 20, 22, 23, 35, 36]. The fact that we measure dipoles is a manifestation that we live in an inhomogeneous universe, not in a smooth background universe, and the subtleties associated with gauge choice in interpreting the cosmic dipole measurements are inevitable. Here we clarify common misunderstanding in the literature associated with the cosmic dipole measurements. However, keep in mind that these subtleties only exist in the theoretical interpretations, not in the measurements themselves.

### A. Relative velocities

In special relativity, the absolute velocity of any object has no physical meaning, and only the velocity relative to an observer (or relative velocity) is physically meaningful. In general relativity, a comparison of two velocities is meaningful only at the same position, as a parallel transport of velocities to a different position is path-dependent. So, the relative velocity from two different spacetime positions has no physical meaning either. In the context of cosmological perturbation

theory, individual velocities are gauge-dependent, and they change their values depending on a coordinate choice. Hence, these individual velocities cannot be associated with any of the dipole measurements, and the only physically meaningful velocity is the gauge-invariant relative velocity at the same spacetime position. The observed dipoles from large-scale structure surveys are indeed measurements of the relative velocities at the same spacetime position, i.e.,

$$\mathbf{v}_{\text{CMB}} = \mathbf{v}_\gamma - \mathbf{v}_o, \quad \mathbf{v}_{\text{LSS}} = \mathbf{v}_g - \mathbf{v}_o, \quad (1)$$

where  $\mathbf{v}_\gamma$ ,  $\mathbf{v}_g$ ,  $\mathbf{v}_o$  are the velocities of the CMB photon fluid, the galaxy sky map, and the observer, and  $\mathbf{v}_{\text{CMB}}$ ,  $\mathbf{v}_{\text{LSS}}$  are the velocities inferred by using the dipole measurements from the CMB anisotropies and the large-scale structure probes (quasars and supernovae are collectively referred to as galaxies with  $\mathbf{v}_g$ ). We clarify the meaning of  $\mathbf{v}_g$  at the observer position in Section II C.

Note that while the individual velocities  $\mathbf{v}_\gamma$ ,  $\mathbf{v}_g$ ,  $\mathbf{v}_o$  are gauge-dependent, the relative velocities  $\mathbf{v}_{\text{CMB}}$  and  $\mathbf{v}_{\text{LSS}}$  are gauge-invariant, as the gauge transformation of the two individual velocities at the same position is cancelled. Hence, the relative velocities are physically meaningful, but the individual velocities are of less physical significance. For instance, popular Boltzmann codes (CMBFAST [37], CAMB [27], CLASS [28]) adopt the synchronous and dark-matter comoving gauge, i.e.,  $\mathbf{v}_o^{\text{sync}} \equiv 0$ , if we assume that the observer is (co-)moving together with dark matter. With this gauge condition, the observer is not moving at all, and the relative velocities from the dipole measurements are  $\mathbf{v}_{\text{CMB}} = \mathbf{v}_\gamma^{\text{sync}}$  and  $\mathbf{v}_{\text{LSS}} = \mathbf{v}_g^{\text{sync}}$ , where we used the superscript to indicate that the quantities are evaluated in the synchronous-comoving gauge. Of course, the values of  $\mathbf{v}_{\text{CMB}}$  and  $\mathbf{v}_{\text{LSS}}$  are independent of gauge choice.

Viewed this way, the observed dipoles from the CMB and the galaxy surveys are not directly related to each other, as they are two different relative velocities with only the observer velocity in common. It is, however, possible that they *happen* to be similar to each other — For example, if the observer velocity is the dominant contribution in a certain gauge, say, the conformal Newtonian (cN) gauge:

$$|\mathbf{v}_o^{\text{cN}}| \gg |\mathbf{v}_\gamma^{\text{cN}}|, \quad |\mathbf{v}_o^{\text{cN}}| \gg |\mathbf{v}_g^{\text{cN}}|, \quad (2)$$

we could then obtain

$$\mathbf{v}_{\text{CMB}} \simeq \mathbf{v}_{\text{LSS}} \simeq -\mathbf{v}_o^{\text{cN}}. \quad (3)$$

Note that a gauge choice is a matter of convenience and any gauge choices are equivalent, such that with other gauge conditions the numerical values of individual velocities  $\mathbf{v}_\gamma$ ,  $\mathbf{v}_g$ ,  $\mathbf{v}_o$  will be different, but the numerical values of the relative velocities ( $\mathbf{v}_{\text{CMB}}$ ,  $\mathbf{v}_{\text{LSS}}$ ) are invariant, i.e.,

$$-\mathbf{v}_o^{\text{cN}} \simeq \mathbf{v}_\gamma^{\text{sync}} \simeq \mathbf{v}_g^{\text{sync}}, \quad (4)$$

if Eq. (2) is valid. In the synchronous gauge, the observer and the dark matter velocities are set zero by a gauge choice, which then shifts all the other velocities, compared to those in

the conformal Newtonian gauge. It is now clear that the peculiar motion of the observer quoted in the literature indeed corresponds to  $\mathbf{v}_{\text{CMB}}$  and  $\mathbf{v}_{\text{LSS}}$ , not  $\mathbf{v}_o$  itself. But with inequalities in Eq. (2), the observed peculiar motion  $\mathbf{v}_o^{\text{CN}}$  in the conformal Newtonian gauge inferred from the dipole measurements would then be the same as in Eq. (3).

### B. No common cosmic rest frames

Furthermore, Eq. (1) makes it clear that the rest frames of CMB and galaxies, in which an observer would see no dipole (or no spatial energy flux), are not unique, but position-dependent, as all individual velocities are a function of space-time position  $x^\mu$ . The rest frames can be unique and shared by all the observers and sources in a background universe with perfect homogeneity and isotropy, but in a real universe with inhomogeneities no common rest frames exist. In this respect, there exist no fundamental observers or “comoving observers” either, who by implicit definition see no dipole of the CMB, galaxies, and any other sources.

In particular, the term “comoving” is often misused in the literature this way, but a comoving observer simply implies that the observer is “co-moving” with a certain fluid, such that the observer sees no dipole of that fluid but the observer can measure dipoles of other fluids. A comoving observer is also used to refer to an observer stationary with respect to comoving coordinates. A better name for this observer would be a coordinate observer, because, in contrast with an observer comoving with a fluid, a coordinate observer simply represents a coordinate system, not associated with any physical quantity. For instance, a normal observer  $n^\mu$  in the Arnowitt-Deser-Misner formalism (ADM; [38]) is an example of a coordinate-dependent observers (see [39] for discussion of various observers and gauge choices).

Because there is only one observer (us) at our position, there is an approximate rest frame in which we see no dipoles from CMB, galaxies, and any other sources, as long as the inequality in Eq. (2) is valid for all the large-scale structure probes. In this regard, this rest frame is unique for all sources, relative to the observer at our position. We show that in the standard cosmology the inequality is satisfied for sources at redshift  $z \gg 0.5$ , but not in the local neighborhood. Furthermore, note that these individual velocities  $\mathbf{v}_\gamma^{\text{CN}}$ ,  $\mathbf{v}_g^{\text{CN}}$  in the conformal Newtonian gauge are never zero in an inhomogeneous universe even at high redshift, but just numerically small compared to  $\mathbf{v}_o^{\text{CN}}$ . Hence the “cosmic rest frame”, even when confined to the only one observer at one spacetime position, is only an approximate one.

### C. Intrinsic velocities and dipoles

What are the individual velocities  $\mathbf{v}_\gamma$ ,  $\mathbf{v}_g$  of the CMB and galaxies at the observer position? To a good approximation, CMB photons we measure today originate from the last scattering surface at  $z_*$ , such that the CMB sky map has much information about the Universe when it was just 370 thousand

years old [9]. However, the CMB sky map itself is indeed a photon fluid *today at the observer position* (in fact more than a fluid, as it possesses higher multipoles), and that is why we can measure it! Collectively as a fluid, the CMB photons form a CMB fluid velocity  $\mathbf{v}_\gamma$  at the observer position in a given choice of coordinate, while the individual photons move at the speed of light.

In the same way, galaxy surveys provide the galaxy number density  $n_g^{\text{obs}}(z, \hat{n})$  as a function of the observed redshift  $z$  and angle  $\hat{n}$ , or one can construct the galaxy sky map  $\Sigma_g^{\text{obs}}(\hat{n})$  by projecting along the line-of-sight direction as in the CMB temperature map. It is well known that the density fluctuation [40] and the redshift-space distortion [4] are the dominant contributions at redshift  $z$  of the source galaxies, but again the observed galaxy maps (either three-dimensional or projected two-dimensional) are indeed physical observables *today at the observer position*, which defines a velocity  $\mathbf{v}_g$  of the observed source galaxies at the observer position in a given choice of coordinate.

These velocities  $\mathbf{v}_\gamma^{\text{CN}}$  and  $\mathbf{v}_g^{\text{CN}}$  are often in the literature referred to as the *intrinsic dipoles*, as they contribute to the dipole measurements. However, as we elaborate below, the “intrinsic dipole” is misleading in many ways. For example, if we boost the observed CMB anisotropies with the relative velocity  $\mathbf{v}_{\text{CMB}}$  we obtain from the CMB dipole measurements, there will be no further dipole anisotropies in the boosted frame (i.e., the rest frame of CMB indeed), rather than we see the residual dipole from the *intrinsic dipole* (see, e.g., [41] for the discussion of the intrinsic dipole of CMB temperature anisotropies). These velocities  $\mathbf{v}_\gamma^{\text{CN}}$  and  $\mathbf{v}_g^{\text{CN}}$  are in a sense *intrinsic* to the observed sources, such that they may better be referred to as *intrinsic velocities* of the sources (at the observer position). We clarify further in Sections III and V with equations for  $\mathbf{v}_\gamma^{\text{CN}}$  and  $\mathbf{v}_g^{\text{CN}}$ .

### D. Bulk velocity flows

Measurements of peculiar velocities are in general difficult, but there exist a few ways to measure the peculiar velocities in the local neighborhood (see, e.g., [42, 43] and the references therein). In particular, measurements of the luminosity distance from supernova observations in the local neighborhood provide a way to directly estimate the peculiar velocity of their host galaxies. With these measurements of the peculiar velocities, the bulk velocity flow can be measured [42, 44–46] by averaging the peculiar velocities over the volume with weights chosen to optimize the signal-to-noise ratio. Anomalous large amplitudes of the bulk flows [42, 46, 47] pose another challenge in the standard  $\Lambda$ CDM cosmology, and there have been attempts [48] to explain the observations in terms of large-scale or super-horizon scale fluctuations.

As we show in Section IV, these measurements of the peculiar velocities are measurements of the relative velocity  $\mathbf{v}_{\text{bulk}} := \mathbf{v}_s - \mathbf{v}_o$  of the source and the observer, not the individual peculiar velocity  $\mathbf{v}_s$  of the sources. Here again note that the individual velocity  $\mathbf{v}_s$  and the observer velocity  $\mathbf{v}_o$  alone are gauge-dependent and they are not physical. Further

averaging over the volume of  $v_{\text{bulk}}$  results in the relative velocity between the observer and the averaged sources. It is then evident that the presence of any fluctuations on scales larger than the averaged volume or the separation between the sources and the observer cannot affect the relative velocity measurements (hence the bulk flow), as both the velocities are affected by such large-scale fluctuations (see [49–51] for the absence of infrared effects on the luminosity distance). The only way to avoid this conclusion is the existence of fluctuations or forces that treat the sources and the observer differently, as opposed to gravity that affects equivalently all the matter components at the same position.

### E. Cosmological principle on large scales

The cosmological principle states that the Universe is homogeneous and isotropic on large scales (see [52, 53]). This statement can be confusing in many ways: at what scale does the Universe become homogeneous and isotropic? how do we average the Universe to recover the homogeneity and isotropy? to what level of fractional deviation does the Universe become homogeneous and isotropic? The cosmological principle is often invoked in the literature for the Ellis & Baldwin test. Here we clarify a few subtleties associated with the cosmological principle in the literature.

First, the cosmological principle provides a way to derive the solution in the nonlinear Einstein equation, i.e., the Robertson-Walker metric and the Friedmann equation, both of which form a background solution. In a background universe, the universe is homogeneous and isotropic on *all* scales. With a background solution, we model the real Universe with inhomogeneities [29–31], by treating the deviations from a background solution as perturbations to the background universe we chose (or cosmological model parameters), which allows us to derive perturbative solutions to the Einstein equation in the real Universe. Hence the cosmological principle is to some degree equivalent to a background solution and tests of the cosmological principle in practice should be performed as tests of our cosmological model predictions that include not only the background evolution but also the perturbation calculations such as CMB power spectrum and so on. Note that with inhomogeneities the real Universe is not homogeneous or isotropic on any scales up to the level of perturbations.

Averaging in cosmology in a hyper-surface of a constant time is known to be gauge-dependent [54, 55], i.e., one obtains different results, depending on our choice of coordinates, along which we average. Furthermore, beyond the linear order in perturbations we never restore the background solution upon averaging, though the so-called back-reaction is shown to be small in the conformal Newtonian gauge (see, e.g., [56–58]). As coordinate averages in a hyper-surface are unphysical and gauge-dependent, we need to provide theoretical descriptions that naturally match the observational procedure, i.e., averages over the light cone in terms of the observed angle and redshift (see, e.g., [59–61]).

Of particular interest in this work is the cosmic dipole measurements, i.e., averages over the observed angular direction

of CMB temperature anisotropies and galaxy samples. As we show in Sections III–V, these large-scale structure probes have effective distance  $\bar{r}_z$  to the sample at redshift  $z$ , and the dipole measurements yield the fluctuations such as the matter density fluctuation for galaxy clustering at  $k \sim 1/\bar{r}_z$ , such that by using galaxy samples at higher redshift or CMB temperature anisotropies we probe larger scales, at which the fluctuations are smaller than our peculiar motion at  $\bar{r} = 0$ , while at lower redshift ( $z \ll 0.5$ ) the dipole measurements can be dominated by fluctuations other than our peculiar motion. The statement that once averaged over large scales we can recover the homogeneity and isotropy and hence the dipole measurements yield our motion is an approximate, but not an accurate description.

### III. DIPOLE FROM CMB ANISOTROPIES

The sky of the cosmic microwave background is nearly isotropic at the level of  $10^{-5}$ , but our motion relative to the CMB rest frame (or the relative velocity  $v_{\text{CMB}} \sim 10^{-3}$ ) induces a dipole anisotropy an order-of-magnitude larger in amplitude than anisotropies on other angular multipoles. The CMB dipole was first discovered [62] in late 1960s and later measured with higher precision by satellite experiments [6–9]. The relative motion between the observer and the CMB rest frame generates not only the Doppler boost of the CMB temperature [8, 63, 64], but also the aberration of the photon directions. The aberration effect can be measured by the change in the angular power spectrum on large multipoles [8, 65, 66], but its impact is small, compared to the change in the dipole. Here we focus only on the computation of the CMB dipole ( $l = 1$ ).

CMB temperature anisotropies on low angular multipoles can be accurately described by a simple analytic formula [67], obtained by assuming 1) the tight coupling of the baryon and the photon fluids before the recombination, 2) an instantaneous recombination at  $T_*$  set by atomic physics, 3) the free-streaming of photons after the recombination. The observed CMB temperature anisotropies along the observed angular direction  $\hat{n}$  are at the linear order in perturbations [68]

$$\begin{aligned} \Theta_\gamma^{\text{obs}}(\hat{n}) = & \Theta_\star - \delta z_\star = \Theta_\star^{\text{cN}} + \mathcal{H}_0 v_{\bar{o}} + \psi_\star - \psi_{\bar{o}} \\ & + (\partial_{\parallel} v)_\star - (\partial_{\parallel} v)_{\bar{o}} + \int_0^{\bar{r}_\star} d\bar{r} (\psi - \phi)', \end{aligned} \quad (5)$$

where  $\Theta$  is the (dimensionless) photon temperature fluctuation,  $\delta z$  is the fluctuation in the observed redshift defined by  $T_\star/T(\hat{n}) =: 1 + z_{\text{obs}}(\hat{n}) = (1 + z_\star)(1 + \delta z)$ , and the subscripts indicate that the field is evaluated at  $\eta_\star$  along the light cone or at the observer position  $\bar{o}$ . In the second equality, we expressed the equation in the conformal Newtonian gauge. The observed CMB temperature anisotropies are essentially the temperature fluctuation  $\Theta_\star$  at the recombination and the relativistic effects  $\delta z_\star$  along the propagation such as the Sachs-Wolfe effect  $\psi$ , the line-of-sight Doppler effect  $\partial_{\parallel} v$ , and the integrated Sachs-Wolfe effect [67] along the line-of-sight direction to the decoupling  $\bar{r}_\star = 13.875$  Gpc at  $z_\star =$

1088 (see Appendix A for our notation convention). Only the scalar contributions are considered here. The analytic formula based on the aforementioned approximations has been widely used in the literature to understand the CMB temperature anisotropies, and the analytic formula matches perfectly the numerical output from the Boltzmann codes on low angular multiples [67–72]. The gauge-invariance of the monopole fluctuation in the observed CMB temperature anisotropies was first proved in [68] by using Eq. (5).

Given the analytic expression in Eq. (5) and its angular decomposition with the multipole moments  $a_{lm}$

$$\Theta_{\gamma}^{\text{obs}}(\hat{n}) = \sum a_{lm} Y_{lm}(\hat{n}), \quad (6)$$

the dipole moment  $a_{1m}$  and its power spectrum  $C_1^{\text{CMB}}$  can be readily computed as

$$C_1^{\text{CMB}} = \langle |a_{1m}|^2 \rangle = 4\pi \int d\ln k \Delta_{\mathcal{R}}^2(k) |\mathcal{T}_1^{\text{CMB}}(k)|^2, \quad (7)$$

with the dipole transfer function [68]

$$\begin{aligned} \mathcal{T}_1^{\text{CMB}}(k) = & [\mathcal{T}_{\Theta^{\text{cN}}}(\eta_{\star}) + \mathcal{T}_{\psi}(\eta_{\star})] j_1(k\bar{r}_{\star}) + k\mathcal{T}_{v_{\gamma}^{\text{cN}}}(\eta_{\star}) j_1'(k\bar{r}_{\star}) \\ & - \frac{1}{3}k\mathcal{T}_{v_m^{\text{cN}}}(\eta_{\bar{0}}) + \int_0^{\bar{r}_{\star}} d\bar{r} [\mathcal{T}_{\psi'}(\eta) - \mathcal{T}_{\phi'}(\eta)] j_1(k\bar{r}), \end{aligned} \quad (8)$$

where  $\mathcal{T}_{\delta p}$  is the transfer function (we suppressed the  $k$ -dependence) for the individual perturbation variable  $\delta p$  defined as  $\delta p(\mathbf{k}, \eta) = \mathcal{T}_{\delta p}(k, \eta) \mathcal{R}(\mathbf{k})$  in terms of the comoving-gauge curvature perturbation  $\mathcal{R}(\mathbf{k})$  in the initial condition, and  $\Theta^{\text{cN}}$ ,  $v_{\gamma}^{\text{cN}}$ ,  $v_m^{\text{cN}}$  represent the CMB temperature fluctuation, the photon velocity potential, and the matter velocity potential in the conformal Newtonian gauge. The derivation of the dipole transfer function is presented in Appendix A. Here we assumed that the observer motion is the same as the matter motion.

Equation (8) reveals that the contribution from the observer motion  $v_m^{\text{cN}}$  has no spherical Bessel function, as it arises from the observer position ( $\bar{r} \equiv 0$ ). The other contributions arising from the position at  $\bar{r}_{\star}$  contain not only their intrinsic angular momentum (e.g., scalar for  $\psi$ , vector for  $v_{\gamma}^{\text{cN}}$ ), but also the orbital angular momentum from  $\exp[i\mathbf{k} \cdot \mathbf{x}]$ . The presence or the absence of the spherical Bessel function is critical in determining which component contributes the most to the dipole transfer function, as the presence of the spherical Bessel function suppresses the individual transfer functions:  $j_l(x) \approx 1/x$  at large  $x$ . This structure in the dipole transfer function is identical to the dipole transfer function for the luminosity distance fluctuations in Section IV and for the galaxy surveys in Section V.

The dipole transfer function  $\mathcal{T}_1^{\text{CMB}}$  in the conformal Newtonian gauge has the contribution  $(-k\mathcal{T}_{v_m^{\text{cN}}}/3)$  from the peculiar motion of the observer (or matter), and the remaining contributions from everything else in Eq. (8) (or everything in Eq. [5] except  $\partial_{\parallel} v$  at the observer position) can be lumped together to define the *intrinsic velocity*  $v_{\gamma}^{\text{cN}}$  of the CMB photon fluid at the observer position today:

$$\mathcal{T}_1^{\text{CMB}}(k) =: \frac{1}{3}k \left[ \mathcal{T}_{v_{\gamma}^{\text{cN}}}(k, \eta_{\bar{0}}) - \mathcal{T}_{v_m^{\text{cN}}}(k, \eta_{\bar{0}}) \right], \quad (9)$$

where the numerical factor 1/3 in  $\mathcal{T}_1^{\text{CMB}}$  arises due to equal contributions from each  $m$ -modes of the dipole ( $l = 1$ ) and also note that the velocity potential is related to the velocity vector as  $\mathbf{v} = -\nabla v$ . The intrinsic velocity potential  $v_{\gamma}$  of the CMB photon fluid at the observer position today defined above indeed gauge transforms like a velocity potential, and hence the difference in two velocity potentials at the same position (or the relative velocity) is gauge-invariant. As discussed in Section II C, this shows that the dipole power is just a measurement of the relative velocity of the observer and the CMB fluid today at the observer position.

This argument is further borne out by the fact that the dipole is related to the spatial energy flux of the CMB photon fluid measured by the observer. Measurements of CMB temperature anisotropies  $\Theta_{\gamma}^{\text{obs}}(\hat{n})$  yield the full information about the distribution function at the observer position

$$f_{\gamma}^{\text{obs}}(\hat{n}) = -\frac{d\bar{f}}{d\ln q} \Theta_{\gamma}^{\text{obs}}(\hat{n}), \quad (10)$$

and thereby the observed energy-momentum tensor of the CMB photon fluid

$$T_{\text{obs},\gamma}^{ab} = 2 \int d^3 E_{\gamma} \frac{E_{\gamma}^a E_{\gamma}^b}{E_{\gamma}} f_{\gamma}^{\text{obs}}(\hat{n}), \quad (11)$$

where  $\bar{f}$  is the Planck distribution,  $q = aE_{\gamma}$  is the photon comoving momentum,  $E_{\gamma}^a = E_{\gamma}(1, -\hat{n})$ , and  $a, b = t, x, y, z$  are the internal coordinates in the observer rest frame with the Minkowski metric (see [73] for the tetrad formalism). In particular, the spatial energy flux measured in the rest frame of the observer

$$T_{\text{obs},\gamma}^{0i} = s^i = (\bar{\rho} + \bar{p})_{\gamma} v_{\text{CMB}}^i, \quad (12)$$

is related to the dipole moment  $a_{1m}$  as

$$v_{\text{CMB}}^i = \sqrt{\frac{3}{4\pi}} \left( \frac{a_{1,-1} - a_{11}}{\sqrt{2}}, i \frac{a_{1,-1} + a_{11}}{\sqrt{2}}, a_{10} \right), \quad (13)$$

where the multipole coefficients are defined in Eq. (6).

In the  $\Lambda$ CDM model the contribution of the intrinsic velocity  $v_{\gamma}^{\text{cN}}$  to the dipole power is negligible ( $\sim 10^{-4}$ ), compared to the kinematic dipole contribution from  $v_{\text{obs}}^{\text{cN}}$ . However,  $v_{\gamma}^{\text{cN}}$  is non-vanishing and differs at each position, such that no unique rest frame of CMB shared by all the observers exists. Also note that what we can obtain from the CMB dipole measurements is only the relative velocity of the observer and the CMB photon fluid, not the observer motion  $v_{\text{obs}}^{\text{cN}}$  in the conformal Newtonian gauge. Hence, when we boost the observed CMB anisotropies with the relative velocity we obtain from the CMB dipole measurements, there exist no further dipole anisotropies from the intrinsic velocity, i.e., the rest frame indeed, and the *intrinsic* dipole is a misnomer.

Figure 1 shows the transfer functions  $\mathcal{T}_{\delta p}$  in Eq. (8). The gravitational potential contributions  $\psi$  today (dashed) and at the recombination (green dashed) are constant on large scales, but decay on small scales. Its time evolution from the recombination epoch until today is very small, mostly arising from

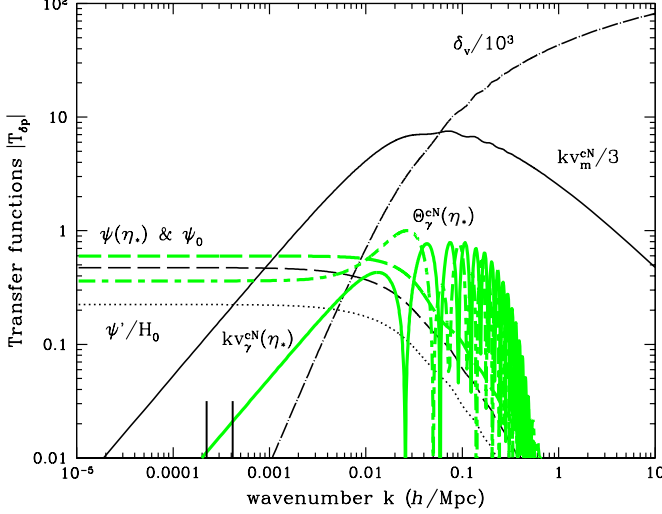


FIG. 1. Transfer functions  $\mathcal{T}_{\delta p}$  for the individual contributions to the dipole power spectra in Eqs. (8), (23), (39). Green curves show the transfer functions at the decoupling epoch  $z_*$ , and they oscillate on small scales, while the other curves show the transfer functions at  $z = 0$ . The gravitational potential changes little over time ( $\psi_*$ ,  $\psi_0$ ), but the growth of the velocity potential is significant. None of the contributions to the transfer function is comparable to the matter density fluctuation  $\delta_v$  in the comoving gauge (dot-dashed). Two short vertical lines indicate the peak positions  $x = 2.08$  and  $x = 3.87$  for  $j_1(x)$  and  $j_1'(x)$  with  $x = k\bar{r}_*$ , beyond which the transfer functions are suppressed by the spherical Bessel function, except the contribution of the observer motion (solid) without the spherical Bessel function. Note that only the individual transfer functions are plotted here, not including the spherical Bessel function contribution. At lower redshift, the peak positions are shifted to higher wave numbers.

the epoch of  $\Lambda$ -domination, as shown by  $\psi'/H_0$  (dotted). The temperature fluctuation  $\Theta_\gamma^{cN}$  (green dot dashed) in the conformal Newtonian gauge is  $2/3$  of the gravitational potential on large scales, but exhibits acoustic oscillations on small scales. The velocity contribution  $kv_\gamma^{cN}$  of the photon fluid at the recombination (green solid) falls as  $k$  on large scales with the velocity potential being constant, while it also oscillates on small scales. The velocity contribution  $kv_m^{cN}/3$  of the observer today (solid) has no significant oscillations as assumed to be the matter component, and it is significantly larger in amplitude as it has grown from the recombination epoch until today by a factor 28, or the ratio of  $\mathcal{H}fD$  at two epochs, where  $\mathcal{H}$  is the conformal Hubble parameter,  $D$  is the growth factor, and  $f$  is the logarithmic growth rate. Note the absence of the spherical Bessel function in  $\mathcal{T}_1^{CMB}$  in Eq. (8) for the observer motion. Hence no suppression due to the spherical Bessel function for the observer motion.

Given that the dipole power  $C_1^{CMB}$  in Eq. (7) is an integral over the dipole transfer function  $\mathcal{T}_1^{CMB}(k)$  in log space with the scale-invariant power spectrum  $\Delta_{\mathcal{R}}^2(k)$ , one can read off the contributions of the individual components in Figure 1 to the dipole power. Most of the dipole power comes from the observer motion (solid), and the remaining 0.01% of the

dipole power comes from the other effects. The presence of the spherical Bessel function  $j_1(x)$  with argument  $x = k\bar{r}_*$  further suppresses all the contributions on small scales ( $x$  larger than the vertical lines), except the contribution of the observer motion. The spherical Bessel functions appear because we expanded plane waves  $e^{ik \cdot x}$  into those with definite angular momentum, and hence no such suppression for any contributions at the observer position  $x_0 = 0$ . The CMB monopole also has contributions at the observer position from the gravitational potential [68], but as evident in Figure 1 those contributions are small. On large scales  $x \ll 1$  with  $j_1(x) \simeq x/3$ , all the contributions add up to cancel the observer motion, such that the full dipole transfer function  $\mathcal{T}_1(k)$  is proportional to  $k^3$  on large scales.

Now we perform numerical computations in the standard  $\Lambda$ CDM cosmology. Given the dispersion in the relative velocity

$$\sigma_{v_{CMB}}^2 := \langle \mathbf{v}_{CMB} \cdot \mathbf{v}_{CMB} \rangle = \int d \ln k \Delta_{\mathcal{R}}^2(k) k^2 \mathcal{T}_{v_{CMB}}^2, \quad (14)$$

the CMB dipole power is related to the relative velocity dispersion as

$$C_1^{CMB} = \frac{4\pi}{9} \sigma_{v_{CMB}}^2 = 4.51 \times 10^{-6}, \quad (15)$$

where  $\sigma_{v_{CMB}} = 1.8 \times 10^{-3} = 540 \text{ km s}^{-1}$ . Assuming that the relative velocity is Gaussian distributed with the velocity dispersion  $\sigma_{v_{CMB}}^2$ , the Maxwell-Boltzmann distribution can be used to derive the mean speed of the relative velocity and its rms deviation from the mean:

$$\bar{v} := \langle |\mathbf{v}_{CMB}| \rangle = \sqrt{\frac{8}{3\pi}} \sigma_{v_{CMB}} = 496 \text{ km s}^{-1}, \quad (16)$$

$$\sigma_{\bar{v}} := \langle (v_{CMB} - \bar{v})^2 \rangle^{1/2} = 212 \text{ km s}^{-1}. \quad (17)$$

The Planck measurements of the CMB dipole yields the relative velocity [8]

$$v_{CMB} = 369 \pm 0.9 \text{ km s}^{-1}, \quad (18)$$

along the constellations of Crater and Leo ( $l, b = (263.99^\circ \pm 0.14^\circ, 48.26^\circ \pm 0.03^\circ)$ ), which is a bit lower than the mean relative velocity  $\bar{v}$ , but well within  $1\text{-}\sigma$  range. Correcting the motion of our Solar system around the Galactic center and assuming that  $v_\gamma^{cN}$  is constant over the shift in the spatial positions, the relative velocity of the CMB fluid and our Galaxy becomes

$$v_{CMB} = 627 \pm 22 \text{ km s}^{-1}, \quad (19)$$

along the direction ( $l, b = (276^\circ \pm 3^\circ, 33^\circ \pm 3^\circ)$ ), which is again well within  $1\text{-}\sigma$  range.

#### IV. DIPOLE FROM SUPERNOVA OBSERVATIONS

The luminosity distances from distant SNIa provides a powerful way to probe cosmological models (see, e.g., [74, 75]).

In addition to the redshift-distance relation in the background, the luminosity distances also fluctuate due to the perturbations in the inhomogeneous Universe. These fluctuations can also be used to measure the dipole [34, 76, 77], in the same way as the CMB dipole is measured. The analysis of supernova light curves for the luminosity distances is often performed by using a compilation of the supernova observations such as the Pantheon+SH0ES data-set [78–80]. Furthermore, measurements of the luminosity distances in the local neighborhood are also used to construct the “background cosmological redshift  $z_{\text{cos}}$ ”, which can be subtracted from the observed redshift to measure the peculiar velocities [81] (see, e.g., [82–86] for recent measurements).

Here we investigate what contributes to the dipole in the luminosity distance measurements and to the peculiar velocity measurements in the local neighborhood.

### A. Luminosity distance fluctuations

With the standardization process, measurements of individual supernovae yield the luminosity distances to the host galaxy at the observed redshift  $z$  along the direction  $\hat{n}$ :

$$D_L(z, \hat{n}) = \bar{D}_L(z) \left[ 1 + \delta D(z, \hat{n}) \right], \quad (20)$$

where the background luminosity distance is  $\bar{D}_L(z) = (1 + z)\bar{r}_z$  and the dimensionless fluctuation  $\delta D$  of the luminosity distance represents the variation in the observed luminosity

distance  $D_L$  (or the observed angular diameter distance  $D_A$ ) due to inhomogeneities in the Universe. The fluctuation  $\delta D$  in the luminosity distance can be computed by following the geodesic path between the source and the observer and by computing the physical area as [34, 87–93]

$$\delta D = \delta z + \frac{\delta r}{\bar{r}_z} - \kappa + \frac{1}{2} (\mathcal{C}_\alpha^\alpha - \mathcal{C}_\parallel), \quad (21)$$

where  $\delta z$  is again the fluctuation in the observed redshift,  $\kappa$  is the lensing convergence,  $\delta r$  is the distortion in the radial position at the observed redshift, and the remaining terms represent the gravitational potential contributions at the source position. We follow the notation convention in [94–96] (see also Appendix A). The lensing convergence and the radial distortion affect the luminosity distance (or the angular diameter distance) by changing the flux (or the physical area), given the observed redshift and angle. The full expression at the linear order in perturbations is composed of three distinct contributions: contributions at the source position, at the observer position, and along the line-of-sight direction, each of which is essential to ensure that the full expression is gauge-invariant [49, 97].

The fluctuation in the luminosity distance in Eq. (21) can be angular decomposed as  $\delta D(z, \hat{n}) = \sum a_{lm}(z) Y_{lm}(\hat{n})$ , and the dipole power  $C_1^{\text{LD}}$  can be computed in the same way as

$$C_1^{\text{LD}}(z) = 4\pi \int d \ln k \Delta_{\mathcal{R}}^2(k) |\mathcal{T}_1^{\text{LD}}(k, z)|^2, \quad (22)$$

with the dipole transfer function for the luminosity distance

$$\begin{aligned} \mathcal{T}_1^{\text{LD}}(k, z) := & -\frac{1}{\mathcal{H}_z \bar{r}_z} \frac{1}{3} k \mathcal{T}_{v_m^{\text{CN}}}(\eta_{\bar{o}}) + \left( \frac{1}{\mathcal{H}_z \bar{r}_z} - 2 \right) \mathcal{T}_\psi(\eta_z) j_1(k \bar{r}_z) + \left( \frac{1}{\mathcal{H}_z \bar{r}_z} - 1 \right) k \mathcal{T}_{v_m^{\text{CN}}}(\eta_z) j_1'(k \bar{r}_z) \\ & + \int_0^{\bar{r}_z} d\bar{r} \left[ \frac{2}{\bar{r}_z} \mathcal{T}_\psi(\eta) - 2 \left( 1 - \frac{1}{\mathcal{H}_z \bar{r}_z} \right) \mathcal{T}_{\psi'}(\eta) + 2 \left( \frac{\bar{r}_z - \bar{r}}{\bar{r}_z \bar{r}} \right) \mathcal{T}_\psi(\eta) \right] j_1(k \bar{r}), \end{aligned} \quad (23)$$

where we again chose the conformal Newtonian gauge for the transfer function computation and assumed that the motion of the observer and the host galaxies for supernova observations follows the matter motion. Similar to the transfer function for the CMB dipole, the transfer function for the luminosity distance dipole consists of contributions from the peculiar motion  $v_m^{\text{CN}}$  and the gravitational potential  $\psi$ . The gravitational lensing effect  $\kappa$  directly contributes to the luminosity distance dipole by changing the observed flux of the source, but not to the CMB dipole due to the spectral measurements.

In contrast to the CMB dipole, the dipole in the luminosity distance receives the contribution from the observer motion  $v_m^{\text{CN}}$  with a coefficient  $1/\mathcal{H}_z \bar{r}_z$ , arising from the contribution in the radial distortion  $\delta r$ , while the contributions of the observer motion in  $\delta z$  and  $\kappa$  cancel (see, e.g., [93, 94, 96]). We can then define the *intrinsic velocity*  $v_{\text{SN}}^{\text{CN}}$  of the “supernova” fluid at the observer position today by collecting all the contributions in the dipole transfer function except the ob-

server motion as

$$\mathcal{T}_1^{\text{LD}}(k, z) =: \frac{1}{\mathcal{H}_z \bar{r}_z} \frac{1}{3} k \left[ \mathcal{T}_{v_{\text{SN}}^{\text{CN}}}(k, \eta_{\bar{o}}) - \mathcal{T}_{v_m^{\text{CN}}}(k, \eta_{\bar{o}}) \right], \quad (24)$$

and hence the dipole power in the luminosity distance fluctuation is then related to the relative velocity as

$$C_1^{\text{LD}}(z) = \frac{4\pi}{9} \frac{\sigma_{v_{\text{LD}}}^2}{\mathcal{H}_z^2 \bar{r}_z^2}, \quad (25)$$

where  $\sigma_{v_{\text{LD}}}^2$  is defined as in Eq. (14) with the relative velocity  $v_{\text{LD}} := v_{\text{SN}} - v_{\bar{o}}$ . Note that only the relative velocity  $v_{\text{LD}}$  is physical, not  $v_{\text{SN}}$  or  $v_{\bar{o}}$ . While the individual components in Eq. (23) are gauge-invariant, the dipole power only measures the relative velocity  $v_{\text{LD}}$ . Since the observed supernova fluid depends on the source redshift  $z$ , we can construct multiple supernova fluids at various redshifts and derive the dipoles as a function of redshift. However, note that these dipoles of the

supernova fluids at various redshifts are the measurements of the relative velocity  $v_{\text{SN}}$  between the observer motion and the supernova fluids at the observer position, exactly in the same way that the expression for the CMB photon fluid in Eq. (8) depends on the decoupling redshift  $z_*$  but the CMB photon fluid we measure is the photon fluid at the observer position. Only the relative velocity at the same position is a physical observable, not the individual velocities.

In practice, the total number of the luminosity distance measurements from individual supernovae ( $\lesssim 2000$ , see, e.g., [98]) is at the moment small for the dipole measurements at multiple redshift slices, such that all the luminosity distance measurements over the whole redshift range can be collected into one sample for the dipole measurement of the full supernova distributions, for which the dipole power is (without the source redshift dependence in  $C_1^{\text{LD}}$ )

$$C_1^{\text{LD}} = 4\pi \int d\ln k \Delta_{\mathcal{R}}^2(k) |\mathcal{T}_1^{\text{LD}}(k)|^2, \quad (26)$$

and the full dipole transfer function

$$\mathcal{T}_1^{\text{LD}}(k) = \int dz \left( \frac{d\bar{N}_{\text{SN}}}{dz} \right) \mathcal{T}_1^{\text{LD}}(k, z), \quad (27)$$

is the integral of the transfer function  $\mathcal{T}_1^{\text{LD}}(k, z)$  at each redshift weighted by the number of individual supernovae, where the redshift distribution  $d\bar{N}_{\text{SN}}/dz$  is normalized to unity. We assumed that the source galaxies for individual supernovae are uniformly distributed, but the source clustering can also contribute to the fluctuations [60, 99]. In this work, we only consider how the individual components in Eq. (23) contribute to the dipole power from the luminosity distance measurements.

Figure 2 shows the individual contributions in Eq. (23) at a given redshift to the dipole power  $C_1^{\text{LD}}$ . With nearly scale-invariant power spectrum  $\Delta_{\mathcal{R}}^2(k)$ , the dipole power in Eq. (22) from the individual components is set by the shape of the transfer functions illustrated in Figure 1 and the characteristic scale  $k \sim 1/\bar{r}_z$  in the spherical Bessel functions. At redshift  $z = 1$ , for instance, the comoving angular diameter distance is  $\bar{r}_z = 3406$  Mpc, and hence the characteristic scales in  $k$  for  $j_1(x)$  and  $j_1'(x)$  at  $z_*$  shown as short vertical lines in Figure 1 are accordingly shifted by the ratio of  $\bar{r}_*/\bar{r}_z = 4.07$  at  $z = 1$ . Roughly speaking, the dipole power in Figure 2 decreases with increasing redshift, simply because the characteristic scales in  $k$  move to larger scales (smaller wave numbers), where the transfer function decreases rapidly.

The dominant contribution in the conformal Newtonian gauge to the dipole power of the luminosity distance fluctuation arises from the observer motion (dashed). In contrast to the case of the CMB, the contribution of the observer motion has a coefficient  $1/\mathcal{H}_z \bar{r}_z$ , arising from the radial distortion  $\delta r/\bar{r}_z$ . The numerical value  $1/\mathcal{H}_z \bar{r}_z$  decreases slowly with redshift from 2.5 at  $z = 0.5$  to 0.7 at  $z = 2.5$ , and its divergence at  $z = 0$  is artificial due to the vanishing luminosity distance at  $z = 0$ . The contribution of the observer motion in CMB without the coefficient is shown as a short horizontal line (solid), and the redshift-dependence in  $C_1^{\text{LD}}$  is entirely due to the coefficient. As pointed out [83, 84], the

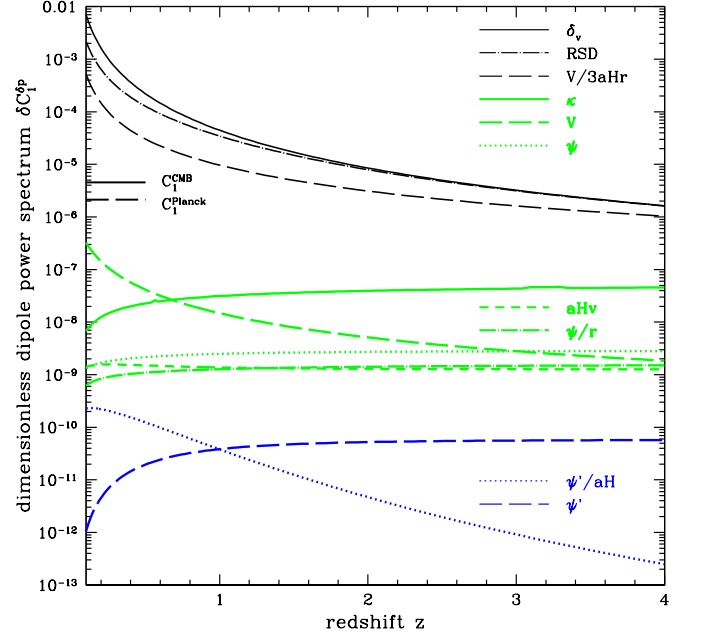


FIG. 2. Dimensionless dipole power spectra from the individual contributions in Eqs. (8), (23), (39). In the dipole transfer functions  $\mathcal{T}_1(k)$ , each transfer function  $\mathcal{T}_{\delta p}(k, \eta_z)$  for the individual contributions  $\delta p$  is multiplied by spherical Bessel functions, and only this product is considered for each curve to compute the dipole power at each redshift  $z$ . From the top to bottom, three curves represent the matter density fluctuation  $\delta_v$  (solid), the redshift-space distortion (dot dashed), the observer motion  $k\mathcal{T}_{v_m^{\text{CN}}}(\eta_0)/3\mathcal{H}\bar{r}_z$  in Eq. (23) (dashed). In the middle, five green curves show the lensing convergence  $\kappa$  (solid), the velocity  $kv_m^{\text{CN}}$  (dashed), the gravitational potential  $\psi$  (dotted), the velocity potential  $\mathcal{H}_z v_m^{\text{CN}}$  (short dashed), and the line-of-sight integration of  $\psi/\bar{r}_z$  (dot dashed). In the bottom, two blue curves show the time derivative of gravitational potential  $\psi'/\mathcal{H}_z$  (dotted) and the line-of-sight integration of  $\psi'$  (dashed). The full dipole power needs to be computed with the full transfer function, which is the sum of all the individual components and integrated over the redshift range, before squared and integrated in Fourier space. All these contributions to the intrinsic velocity of the sources fall as the source redshift increases, while the observer velocity  $v_o^{\text{CN}}$  in the conformal Newtonian gauge remains constant. Two short horizontal lines represent the mean dipole power of CMB (solid:  $C_1^{\text{CMB}} = 4.5 \times 10^{-6}$ ) from our fiducial cosmological model and the dipole power from the Planck measurements (dashed:  $C_1^{\text{Planck}} = 2.1 \times 10^{-6}$ ), which to a good approximation represent the observer velocity  $v_o^{\text{CN}}$  in the conformal Newton gauge.

dipole power in the luminosity distance fluctuation quickly vanishes at high redshift, again due to the redshift-dependent coefficient. One simple way to improve the signal is to weight the individual supernovae with  $\mathcal{H}_z \bar{r}_z$ , before the dipole power is computed.

The other contributions in Eq. (23) are smaller than the contribution from the observer motion by orders of magnitude. The source velocity (green dashed)  $kv_m^{\text{CN}}$  at the source redshift and the lensing convergence  $\kappa$  (green solid) are the next leading contributions to the dipole power. The source velocity

contribution reduces to the observer velocity (short horizontal;  $C_1^{\text{CMB}}$ ) in the limit  $z \rightarrow 0$  as  $j_1'(0) = 1/3$ . As can be inferred in Figure 1, the source velocity transfer function at redshift  $z$  is between solid curve at  $z = 0$  and green solid curve at  $z_*$ , but the suppression from the spherical Bessel function  $j_1'(x)$  reduces its contribution to the dipole power with increasing redshift. This contribution to the CMB dipole can also be estimated by extrapolating the dashed curve in Figure 2 to  $z_*$ , which is orders of magnitude smaller than the contribution of the observer motion. The lensing contribution (green solid) increases with redshift, as it accumulates the fluctuations along the line-of-sight direction. Since the gravitational potential changes so little over time (dashed and green dashed) and its transfer function is flat on large scales shown in Figure 1, the lensing contribution saturates at high redshift. However, as discussed below in detail, the lensing contribution remains unaffected, when we consider the redshift distribution of the sources, while the individual contributions at the source redshift smooth out and decrease.

Three remaining curves in the middle show the other relativistic contributions: the gravitational potential  $\psi$  (green dotted) at the source, the line-of-sight integral of the gravitational potential  $\int d\bar{r} \psi/\bar{r}_z$  (green dot dashed), and the velocity potential  $\mathcal{H}_z v_m^{\text{cN}}$  (green dashed). The latter does not contribute to  $C_1^{\text{LD}}$ , but to  $C_1^{\text{LSS}}$  discussed in Section V. While they are small compared to the contribution of the observer motion, the gravitational potential contribution (dotted) at  $z_*$  is indeed the dominant contribution in the CMB power spectra  $C_{l \neq 1}^{\text{CMB}}$  except for the dipole. The other remaining contributions (blue) shown in the bottom of Figure 2 is even smaller, as the gravitational potential becomes constant soon after the dark energy becomes negligible at high redshift. Given the forecast that the Vera C. Rubin observatory [100] would measure  $N_{\text{SN}} \sim 10^6$  supernovae, the shot-noise for the dipole power is

$$C_{\text{shot}} = \frac{4\pi}{N_{\text{SN}}} \sim 10^{-5}, \quad (28)$$

such that only the velocity (dashed in Figure 2) of the sources at low redshift is relevant, in addition to the observer velocity. Note that the boost factor  $1/\mathcal{H}\bar{r}$  enhances the velocity contributions.

## B. Peculiar velocity measurements

As mentioned, the luminosity distance measurements can also be used as a direct measurement of our peculiar velocity measurements in the local neighborhood [76, 81, 83–86]. At low redshift ( $z \ll 1$ ), the background luminosity becomes

$$\bar{D}_L(z) = (1+z)\bar{r}_z \simeq \frac{z}{H_0}, \quad (29)$$

and the (dimensionless) fluctuation in the luminosity distance becomes [34, 89, 92, 93, 95]

$$\delta D \simeq V_{\parallel}^{\text{cN}} - \frac{1}{\mathcal{H}_z \bar{r}_z} (V_{\parallel}^{\text{cN}} - V_{\parallel, \bar{o}}^{\text{cN}}) \simeq V_{\parallel}^{\text{cN}} - \frac{V_{\parallel}^{\text{cN}} - V_{\parallel, \bar{o}}^{\text{cN}}}{z}, \quad (30)$$

where we ignored all the potential contributions in Eq. (21),  $V_{\parallel}^{\text{cN}}$ ,  $V_{\parallel, \bar{o}}^{\text{cN}}$  are the line-of-sight velocities of the source and the observer in the conformal Newtonian gauge, and  $\mathcal{H}_z \bar{r}_z \simeq z$  at low redshift. Note that the velocity is defined as  $\mathbf{v} = -\nabla v$ , and the line-of-sight velocity is  $V_{\parallel} := \hat{n} \cdot \mathbf{v}$ . Hence the observed luminosity distance in Eq. (20) at low redshift is

$$D_L(z, \hat{n}) \simeq \frac{z + V_{\parallel, \bar{o}}^{\text{cN}} - V_{\parallel}^{\text{cN}}}{H_0}, \quad (31)$$

where we used the low-redshift approximation  $zV_{\parallel}^{\text{cN}} \simeq \mathcal{O}(2)$ . By defining the “cosmological redshift”  $z_{\text{cos}} := H_0 D_L(z, \hat{n})$  for a given choice of the Hubble parameter  $H_0$ , the peculiar velocity of the source can be obtained (if the choice of  $H_0$  is correct) as

$$\Delta z := z - z_{\text{cos}} \simeq V_{\parallel}^{\text{cN}} - V_{\parallel, \bar{o}}^{\text{cN}}, \quad (32)$$

which is in fact the relative velocity between the source and the observer in the conformal Newtonian gauge. Note that the relative velocity is gauge-invariant and with the low-redshift approximation the source and the observer position are essentially the same.

Any velocity flows that shift the source and the observer together cannot be measured, and only the relative motion can be measured, as apparent in Eq. (32). According to the equivalence principle, a uniform shift in the gravitational potential or a uniform shift in the velocity affects both the test particle and the laboratory, leaving no observable trace. While not manifest in Eq. (23), it was shown [49, 51, 101] that any such fluctuations with wavelength larger than the separation between the source and the observer cancel each other in the luminosity distance fluctuations, if we used the full relativistic formula in a  $\Lambda$ CDM universe (the cancellation requires not only the velocity, but also the gravitational potential contributions).

In the local neighborhood, the peculiar velocities of the individual sources can be measured. In particular, the supernova observations are used [42, 46] to estimate the bulk velocity  $\mathbf{v}_{\text{bulk}}$ . While the anomalously large amplitudes in the measurements are odd, the presence of any large-scale fluctuations cannot explain the deviation from the standard  $\Lambda$ CDM model predictions. The relative velocity  $\mathbf{v}_{\text{bulk}}$  of the bulk flow can be altered, only when such fluctuations treat the sources and the observer differently. Even in the presence of isocurvature fluctuations, it is difficult to provide a mechanism to discriminate the observer versus the supernova sources (see [102, 103] for the impact of isocurvature fluctuations on large scales).

## V. DIPOLE FROM GALAXY SURVEYS

Galaxy surveys map the angular positions of distant galaxies, quasars, or any other cosmological sources, in general as a function of its flux (see, e.g., [10, 11]). For galaxy clustering analysis, it is important to have the redshift measurements of the sources. With the Ellis & Baldwin test [5] for the cosmological principle by measuring the dipole from galaxy surveys,

however, the redshift information is not essential, but a large sky coverage of the surveys ( $f_{\text{sky}} \geq 1/2$ ) is critical for the dipole measurements, posing a distinct challenge in modern galaxy surveys. A few, but certainly not many galaxy surveys meet this requirement.

The NRAO VLA Sky Survey (NVSS; [18]) of radio sources is the first large-scale survey, in which the dipole from galaxy surveys is robustly measured [12–17]. Subsequently, other surveys such as 2MASS [104], TGSS [105], SDSS [10] have been used to measure the dipoles [14, 19, 20, 22, 23, 106]. Recently, by using the quasars from the WISE survey [25], a more precise measurement of the dipole was obtained in [21], proving the general trends seen from all the previous measurements that the dipoles from galaxy surveys are largely aligned with the direction of the CMB dipole, but its amplitude is larger by a factor of few, compared to our theoretical expectation of the Ellis & Baldwin formula based on the CMB dipole measurements. The discrepancy in the dipole measurement is now significant at the 5- $\sigma$  level [21]. Here we discuss in detail what contributes to the dipole from galaxy surveys.

A galaxy sample is chosen over a redshift range in a given survey in terms of their properties such as luminosity, morphology, and color. In particular, a constant luminosity threshold over the redshift range (or volume-limited sample) is important to ensure the uniformity of the chosen galaxy sample. For simplicity, we assume that galaxy samples are chosen in terms of a luminosity threshold  $L_t$ . The observed galaxy number counts as a function of the observed redshift  $z$  and angular direction  $\hat{n}$  can then be used to derive the observed galaxy number density:

$$n_g^{\text{obs}}(z, \hat{n}) = \bar{n}_g(z)[1 + \delta_g(z, \hat{n})], \quad (33)$$

and the number density fluctuation  $\delta_g$  at the linear order in perturbations originate from two distinct effects [107]:

$$\delta_g = \delta S + \delta V, \quad (34)$$

where  $\delta S$  represents the contributions associated with the source galaxy population and  $\delta V$  represents the contributions associated with the observed volume.

The dominant source effect is the intrinsic galaxy fluctuation, expressed in terms of the matter density fluctuation  $\delta_v$  in the rest frame of the source galaxies (or the proper time hypersurface [39, 108]) and the galaxy bias factor  $b$  [40], where the subscript  $v$  indicates that the comoving gauge ( $v \equiv 0$ ) is chosen for computing the matter density fluctuation. Two additional contributions in the source effect arise due to our expression of the observed galaxy at the observed redshift  $z$  and the luminosity cut of the sample at the observed redshift, where the evolution bias factor and the magnification bias fac-

tor are defined as

$$e_z := \frac{d \ln \bar{n}_g}{d \ln(1+z)}, \quad t_L := -2 \frac{d \ln \bar{n}_g}{d \ln L}, \quad (35)$$

and two coefficients depend on redshift and the luminosity threshold. Our definition of the magnification bias factor is related to the slope  $s$  of the luminosity function  $d\bar{n}_g/dL \propto L^{-s}$  or the slope  $p$  in terms of magnitude for the cumulative number density  $\log_{10} \bar{n}_g(\leq M) = pM + \text{constant}$  as

$$t_L = 5p = 2(s-1). \quad (36)$$

Hence the source effect is

$$\delta S = b \delta_v - e_z \delta z_v - t_L \delta D, \quad (37)$$

where  $\delta z_v$  is the distortion  $\delta z$  in the observed redshift evaluated in the comoving gauge ( $v \equiv 0$ ) and  $\delta D$  is the fluctuation in the luminosity distance in Eq. (21). If we impose more conditions for selecting galaxies in our sample (for example, galaxy size and shape), there will be additional terms in  $\delta S$ , corresponding to the fluctuation associated with the extra conditions imposed in terms of our observables.

The volume effect  $\delta V$  arises from the distortion in the relation between the observed volume and the physical volume occupied by the observed galaxies, and it can be readily computed by tracing the photon geodesic backward to the source as

$$\delta V = 3 \delta z + \delta g + 2 \frac{\delta r}{\bar{r}_z} - 2\kappa + H \frac{d}{dz} \delta r - \alpha + V_{\parallel}, \quad (38)$$

where  $\delta g$  is the metric determinant and  $V_{\parallel}$  is the line-of-sight velocity (see Appendix A). In contrast to the source effect, the volume effect is independent of how we choose our galaxy samples. The expression in Eq. (38) is derived at the linear order in perturbations, accounting for all the relativistic effects and it was shown [109–113] that the full expression is gauge-invariant. The dominant contributions in the volume effect are the redshift-space distortion [4] in the radial derivative of  $\delta r$  and the lensing effect  $\kappa$  [114]. The factor two of the lensing convergence  $\kappa$  in  $\delta V$  and the term  $t_L \delta D \ni t_L \kappa$  in the source effect are collectively referred to as the lensing magnification bias [114–117].

The observed galaxy number density  $n_g^{\text{obs}}$  at the linear order in perturbations receives contributions from three different types, exactly in the same way as the CMB temperature anisotropies: one from the source position, one from the observer position, and one along the line-of-sight direction. Once we decompose  $\delta_g^{\text{obs}}(z, \hat{n}) = \sum a_{lm}(z) Y_{lm}(\hat{n})$ , the dipole transfer function can be straightforwardly computed as

$$\begin{aligned} \mathcal{T}_1^{\text{LSS}}(k, z) := & \left(1 - h_z + \frac{t_L}{\mathcal{H}_z \bar{r}_z}\right) \frac{k}{3} \mathcal{T}_{v_m^{\text{cN}}}(\eta_{\bar{o}}) + \left[h_z - 3 + t_L \left(1 - \frac{1}{\mathcal{H}_z \bar{r}_z}\right)\right] k \mathcal{T}_{v_m^{\text{cN}}}(\bar{r}_z) j_1'(k \bar{r}_z) + \frac{k^2}{\mathcal{H}_z} \mathcal{T}_{v_m^{\text{cN}}}(\bar{r}_z) j_1''(k \bar{r}_z) \\ & + \left\{ b \mathcal{T}_{\delta_v}(\bar{r}_z) - e_z \mathcal{H}_z \mathcal{T}_{v_m^{\text{cN}}}(\bar{r}_z) + \left[h_z - 4 + t_L \left(2 - \frac{1}{\mathcal{H}_z \bar{r}_z}\right)\right] \mathcal{T}_{\psi}(\bar{r}_z) + \frac{1}{\mathcal{H}_z} \mathcal{T}_{\psi'}(\bar{r}_z) \right\} j_1(k \bar{r}_z) \\ & + \int_0^{\bar{r}_z} d\bar{r} \left\{ \left(\frac{4 - 2t_L}{\bar{r}_z}\right) \mathcal{T}_{\psi}(\bar{r}) + \left[2(h_z - 3) + 2t_L \left(1 - \frac{1}{\mathcal{H}_z \bar{r}_z}\right)\right] \mathcal{T}_{\psi'}(\bar{r}) - 2(t_L - 2) \left(\frac{\bar{r}_z - \bar{r}}{\bar{r}_z \bar{r}}\right) \mathcal{T}_{\psi}(\bar{r}) \right\} j_1(k \bar{r}), \end{aligned} \quad (39)$$

where we again chose the conformal Newtonian gauge and suppressed the  $k$ -dependence in the transfer functions  $\mathcal{T}_{\delta p}$ , and the redshift-dependent coefficient  $h_z$  is defined [118, 119] as

$$h_z := e_z + \frac{2}{\mathcal{H}_z \bar{r}_z} + \frac{\mathcal{H}'_z}{\mathcal{H}_z^2}, \quad \frac{\mathcal{H}'}{\mathcal{H}^2} = 1 + \frac{\dot{H}}{H^2} = -\frac{1}{2} \sum_i (1 + 3w_i) \Omega_i = -\frac{3}{2} \sum_i (1 + w_i) \Omega_i - \Omega_k, \quad (40)$$

with the relation  $1 = \Omega_k + \sum \Omega_i$  and  $w_i$  being the equation of state for individual component. The first contribution  $k \mathcal{T}_{v_m^{\text{cN}}}/3$  is again the contribution of our peculiar motion at the observer position. Evident in Eq. (39), the dipole moment in galaxy surveys *not only* arises from our peculiar motion, *but also* receives contributions from other sources such as the matter density fluctuation  $\mathcal{T}_{\delta_v}$ , the redshift-space distortion  $k^2 \mathcal{T}_{v_m^{\text{cN}}}/\mathcal{H}_z$ , the gravitational lensing  $(\bar{r}_z - \bar{r}) \mathcal{T}_{\psi}/\bar{r}_z \bar{r}$ , and other velocity and relativistic contributions, consisting of three distinct types of contributions, exactly in the same way for CMB in Eq. (8) and the luminosity distance fluctuation in Eq. (23).

In contrast to measuring the three-dimensional clustering of galaxies with the observed galaxy number density  $n_g^{\text{obs}}(z, \hat{n})$ , the dipole measurements in galaxy surveys are performed by collecting all the galaxies in a given redshift range (or projecting along the line-of-sight directions) to construct galaxy sky maps  $\Sigma_g^{\text{obs}}(\hat{n})$ . The number of galaxies in a unit solid angle is  $dN_g(\hat{n}) = \Sigma_g^{\text{obs}}(\hat{n}) d\Omega$ , and the angular number density of galaxies is then related to  $n_g^{\text{obs}}$  as

$$\Sigma_g^{\text{obs}}(\hat{n}) = \int dz \left( \frac{d\bar{V}}{dz d\Omega} \right) n_g^{\text{obs}}(z, \hat{n}), \quad (41)$$

where  $(d\bar{V}/dz d\Omega) = \bar{r}_z^2/H_z(1+z)^3$  is the physical volume element in a unit redshift  $dz$  and a unit solid angle  $d\Omega$  in a background universe and the integration is over the full redshift range of the sample. In the limit the redshift range goes to zero ( $\Delta z \rightarrow 0$ ), the angular number density reduces to the observed galaxy number density at a given redshift  $\Sigma_g^{\text{obs}}(\hat{n}) \propto n_g^{\text{obs}}(z, \hat{n})$ , but the physical volume factor at the same time becomes zero, giving rise to an infinite shot-noise contribution (see Appendix B). Hence the redshift depth should be chosen sufficiently large enough to ensure a reasonable signal-to-noise ratio.

The galaxy sky maps in Eq. (41) can be angular decomposed in the same way as

$$\frac{\Sigma_g^{\text{obs}}(\hat{n})}{\bar{\Sigma}_g} = \sum_{l \geq 1} a_{lm} Y_{lm}(\hat{n}), \quad (42)$$

after removing the background average (angular) number den-

sity

$$\bar{\Sigma}_g := \int dz \left( \frac{d\bar{V}}{dz d\Omega} \right) \bar{n}_g(z). \quad (43)$$

The dipole power  $C_1^{\text{LSS}}$  can then be again computed as

$$C_1^{\text{LSS}} = 4\pi \int d \ln k \Delta_{\mathcal{R}}^2(k) |\mathcal{T}_1^{\text{LSS}}(k)|^2, \quad (44)$$

where we defined the full dipole transfer function

$$\mathcal{T}_1^{\text{LSS}}(k) := \frac{1}{\bar{\Sigma}_g} \int dz \left( \frac{d\bar{V}}{dz d\Omega} \right) \bar{n}_g(z) \mathcal{T}_1^{\text{LSS}}(k, z). \quad (45)$$

While the dipole in the galaxy sky maps is much more complicated than in Eq. (8) of CMB temperature anisotropies or in Eq. (23) of the luminosity distance fluctuations, we can define in the same way the *intrinsic velocity*  $\mathbf{v}_g^{\text{cN}}$  of the galaxy fluid at the observer position today by adding all the contributions in the dipole transfer function  $\mathcal{T}_1^{\text{LSS}}(k)$  except the observer motion as

$$\mathcal{T}_1^{\text{LSS}}(k) =: \mathcal{M} \frac{1}{3} k \left[ \mathcal{T}_{v_g^{\text{cN}}}(k, \eta_{\bar{o}}) - \mathcal{T}_{v_m^{\text{cN}}}(k, \eta_{\bar{o}}) \right], \quad (46)$$

with the coefficient

$$\mathcal{M} := \frac{1}{\bar{\Sigma}_g} \int dz \left( \frac{d\bar{V}}{dz d\Omega} \right) \bar{n}_g(z) \left( h_z - 1 - \frac{t_L}{\mathcal{H}_z \bar{r}_z} \right), \quad (47)$$

and hence the dipole power from galaxy surveys is a measure of the relative velocity as

$$C_1^{\text{LSS}} = \frac{4\pi}{9} \mathcal{M}^2 \sigma_{\text{LSS}}^2. \quad (48)$$

For the moment, if we ignore all the contributions in  $n_g^{\text{obs}}$  except one due to the peculiar motion of the observer (i.e., we ignore the *intrinsic velocity* contribution or the kinetic dipole), the observed angular density of galaxies is then

$$\Sigma_g^{\text{obs}}(\hat{n}) \approx \bar{\Sigma}_g [1 - \mathcal{M}(\partial_{\parallel} v)_{\bar{o}}], \quad (49)$$

and note that the line-of-sight velocity of the observer in the conformal Newtonian gauge is  $V_{\parallel} = \mathbf{V}_{\bar{o}} \cdot \hat{n} = -(\partial_{\parallel} v)_{\bar{o}}$ . Given

the angular dependence of the dipole, the coefficient  $\mathcal{M}$  can be measured from large-scale surveys, and it was shown [120] that this coefficient  $\mathcal{M}$  corresponds to the dipole amplitude of the Ellis-Baldwin test in the absence of redshift evolution (see also [121, 122]). In fact, [123] showed that the correspondence is generally valid even with redshift evolution.

Figure 2 shows the individual contributions in Eq. (39) at the source redshift to the dipole power  $C_1^{\text{LSS}}$ . Each contribution is again computed at a given redshift, and only one contribution is considered in computing the dipole power in Figure 2. Compared to the CMB and the luminosity distance fluctuations, the notable difference in the observed galaxy number density fluctuation in Eq. (39) is the existence of the matter density fluctuation  $\delta_v$  with the galaxy bias factor  $b$ . On large scales, galaxies are biased tracers of the underlying matter distribution [40], and the transfer function for the matter density contribution at  $z = 0$  (dot dashed) in the comoving gauge is larger than any other contributions in Figure 1 by orders of magnitude. Since the transfer function scales as  $\mathcal{T}_{\delta_v} \propto k^2$  on large scales and  $\mathcal{T}_{\delta_v} \propto k^{1/2}$  on small scales, its contribution to the dipole power (solid) in Figure 2 decreases with increasing redshift, again due to the suppression from the spherical Bessel function  $j_1(x)$ , in addition to the decreasing growth factor  $D(z)$ . Note that the linear bias factor is not considered in Figure 2 and it is expected to grow  $b(z) - 1 = (b_0 - 1)/D(z)$  in a simple model [124], where the growth factor is normalized to unity at  $z = 0$ .

As discussed in Section II, the dipole measurements probe the fluctuations in the observed galaxy samples or CMB temperature anisotropies at the characteristic scale  $k \sim 1/\bar{r}_z$ , and the fluctuations from the matter density or the observer motion are never zero at any redshift. At high redshift, the contribution from the observer motion ( $C_1^{\text{CMB}}$ : short horizontal line in Figure 2) dominates over the other contributions, while at low redshift the contribution from the matter density fluctuation is significantly larger than the observer motion [12, 14, 15, 17, 102, 120, 121, 125, 126], even after accounting for the projection over the redshift range (see below). The dipole contribution from the local structure (density fluctuation) is also referred to as local dipole or clustering dipole.

The other interesting contribution to  $C_1^{\text{LSS}}$  is the redshift-space distortion [4] (dot dashed) in Figure 2, which arises from the volume effect with the line-of-sight velocity contribution to the observed galaxy number density fluctuation. Being a spatial derivative of the line-of-sight velocity, the redshift-space distortion is as important as the matter density fluctuation to the three-dimensional clustering of galaxies. However, once the galaxy sky map  $\Sigma_g^{\text{obs}}$  is constructed by collecting all the galaxies along the line-of-sight, the redshift-space distortion contribution to the dipole power is significantly reduced, as the volume effect contributes to the observed galaxy sky map only around the boundary of the redshift range.

Two remaining contributions in Figure 2 that are not yet discussed in  $C_1^{\text{CMB}}$  or  $C_1^{\text{SN}}$  are the velocity potential  $\mathcal{H}_z v_m^{\text{cN}}$  (green short dashed) and the time derivative of the gravitational potential  $\psi'/\mathcal{H}_z$  (blue dotted) in Figure 2. The dimensionless velocity potential is  $\mathcal{H}_z v_m^{\text{cN}} = 1 - 1/\Sigma(z)$  with little

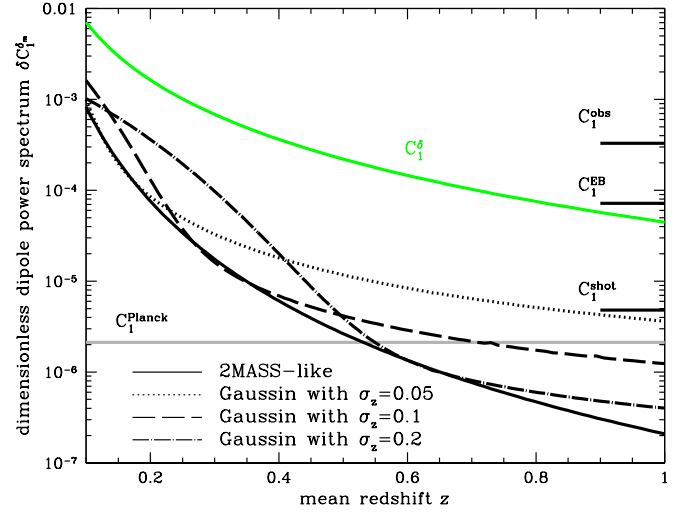


FIG. 3. Dimensionless dipole power spectra from the matter density fluctuations integrated over various redshift distributions. Solid curve shows the dipole power with the distribution in Eq. (52) as a function of the mean redshift  $z$ . The redshift distribution of the Cat-Wise sample is similar to the solid curve with mean redshift  $z = 1$ . Dotted, dashed, and dot-dashed curves show the dipole power with Gaussian redshift distribution in Eq. (51), and the variance for the Gaussian distributions is set  $\sigma_z = 0.05, 0.1$ , and  $0.2$ , respectively. In comparison, the green solid curve shows the dipole power from the matter density fluctuations  $C_1^\delta$  at each redshift slice shown in Figure 2. The density contributions are greatly reduced in amplitude, once averaged over the redshift distributions. Three horizontal lines at  $z = 1$  indicate the observed dipole power  $C_1^{\text{obs}}$  from the CatWise survey, the dipole power  $C_1^{\text{EB}}$  expected from the Ellis-Baldwin formula for the survey, and the shot-noise power. The dipole power from the Planck measurements is shown as the gray horizontal line. Note that the matter density contributions in this plot should be multiplied by the bias factor  $b \approx 2$  and the Ellis-Baldwin coefficient  $\mathcal{M} \approx 6$ , and hence the dipole power  $C_1 \propto b^2 \mathcal{M}^2$  is boosted by  $\approx 140$  for various curves to be compared to the observed dipole power  $C_1^{\text{obs}}$ .

time-dependence [127] in a  $\Lambda$ CDM universe, where  $\Sigma(z) := 1 + 3\Omega_m(z)/2f$  increases from 1.9 at  $z = 0$  to 2.5 in the matter dominated era. The time-derivative of the potential is  $\psi'/\mathcal{H}_z = \psi(f - 1)$ , and it vanishes once  $f \rightarrow 1$  in the matter dominated era. Both effects are negligible contributions to  $C_1^{\text{LSS}}$ .

As mentioned, the individual contributions to the dipole power from galaxy surveys in Figure 2 are illustrative, but not directly observable, due to the infinite shot-noise contributions, arising from the zero volume in a redshift slice with its depth  $\Delta z \rightarrow 0$  (see Appendix B). In real surveys, the source samples for the dipole measurements are constructed by collecting all the galaxies at all redshifts that is brighter than some flux threshold, and it is quite often the case there exist no redshift information for individual galaxies in the sample. Here we numerically compute the contributions of the intrinsic velocity to the dipole power by assuming various redshift distributions of the source galaxies.

Among all the individual contributions to the intrinsic ve-

locity of the sources in Eq. (39), we only consider the contribution of the matter density fluctuation. As evident in Figure 2, the density fluctuation (solid) is the dominant contribution to the dipole power. While the redshift-space distribution (dot-dashed) is comparable to the density fluctuation, their impact is greatly reduced in galaxy samples obtained by integrating over all redshift range, rather than by collecting galaxies in small redshift bins, as the effect originates from the radial distortion in a narrow redshift bin [111]. Arising from the fluctuation along the line-of-sight direction, the contribution of the gravitational lensing (green solid) remains similar in both the redshift-bin and projected samples. Their contribution is, however, several orders of magnitude below the density fluctuations at  $z \leq 2$ , though its contribution indeed dominates at higher redshift.

Figure 3 shows the dipole power from the matter density fluctuations of the sources distributed over various redshift range. The normalized redshift distribution of the galaxy samples is defined as

$$\frac{dN_g}{dz} := \frac{4\pi f_{\text{sky}}}{\bar{\Sigma}_g} \left( \frac{d\bar{V}}{dz d\Omega} \right) \bar{n}_g(z), \quad (50)$$

and we consider two redshift distributions: A simple Gaussian distribution in terms of the mean redshift  $\bar{z}$  and its variance  $\sigma_z$ :

$$\left( \frac{dN_g}{dz} \right)_G = \frac{1}{\sqrt{2\pi}\sigma_z} \exp \left[ -\frac{(z - \bar{z})^2}{2\sigma_z^2} \right], \quad (51)$$

and a more realistic distribution that is used to model the 2MASS observations [14]:

$$\left( \frac{dN_g}{dz} \right)_R = \frac{3z^2}{2(\bar{z}/1.412)^3} \exp \left[ -\left( \frac{z}{\bar{z}/1.412} \right)^{3/2} \right], \quad (52)$$

where the mean redshift ( $1.065\bar{z}$ ) and the peak ( $0.858\bar{z}$ ) of the distribution are given in terms of the parameter  $\bar{z}$ . The former describes the redshift-bin samples, and the latter has the typical power-law distribution combined with an exponential cut-off at high redshift. The CatWise sample [128] is well described by the latter with  $\bar{z} \approx 1$  [21, 121].

The contribution from the matter density fluctuations (green solid curve) in Figure 3 is much larger than the dipole power  $C_1^{\text{Planck}}$  from the observer motion (horizontal gray line; redshift-independent). However, the spherical Bessel function  $j_1(k\bar{r}_z)$  is averaged over a range of redshift with the weight given by  $(dN_g/dz)$  as in Eq. (45), leading to the reduction in amplitude at a given  $k$  and hence the lower dipole power  $C_1$ , compared to the dipole power at each redshift slice (green solid curve). The suppression scale  $k$  is set by the condition  $k\Delta\bar{r}_z \approx \text{few}$ , such that the integration over the redshift range covers a few periods of the oscillations. This argument is indeed borne out by various curves in Figure 3. Three curves (dotted, dashed, and dot-dashed) with the Gaussian redshift distribution show that the dipole power from the matter density fluctuations at a given redshift is reduced by a factor ten (dotted with  $\sigma_z = 0.05$ ) or two orders-of-magnitude (dot-dashed with  $\sigma_z = 0.2$ ) in amplitude. At lower redshift  $\bar{z} \simeq \sigma_z$ , where  $k\bar{r}_z \approx k\Delta\bar{r}_z$ , however, the average over the

redshift range probes the first peak of the oscillations, and hence it adds up, rather than averages out to zero. A similar trend is also shown in the dark solid curve for the 2MASS distribution, which resembles the redshift-bin sample at lower values of  $\bar{z}$  but a broader distribution at higher values of  $\bar{z}$ . In [120], the same conclusion was drawn by using a similar but different parametrization of the redshift distribution.

Analyzing the CatWise samples, it was found [21] that the observed dipole power  $C_1^{\text{obs}}$  is a factor four higher (a factor two in terms of  $\sigma_{\text{LSS}}$ ) than expected dipole power  $C_1^{\text{EB}}$  from the Ellis-Baldwin prediction [21, 102] based on two parameters ( $x \approx 1.7$  and  $\alpha \approx 1.3$ , i.e.,  $\mathcal{M} \approx 6$ ) and the Planck dipole power  $C_1^{\text{Planck}}$ :

$$C_1^{\text{EB}} := \mathcal{M}^2 C_1^{\text{Planck}}. \quad (53)$$

The dipole power  $C_1^\delta \simeq 2 \cdot 10^{-7}$  from the matter density fluctuations at  $\bar{z} = 1$  needs to be further multiplied by the bias factor  $b(z)$  of the samples and the Ellis-Baldwin coefficient  $\mathcal{M}$ , which leads to an approximate factor 140 in  $C_1^\delta$ . Nevertheless, this contribution is still smaller by a factor ten around  $\bar{z} = 1$ , not enough to explain the observed dipole power. The nonlinearity in the matter density fluctuation can significantly boost the contribution (see, e.g., [129]), but only at redshift  $\bar{z} \leq 0.5$ , at which the peak contribution of the matter density fluctuation is at  $k \approx 1/\bar{r}_z \approx 7 \cdot 10^{-4} \text{ hMpc}^{-1}$ .

The shot-noise contribution to the dipole power  $C_1^{\text{shot}}$  also arises, as galaxies are discrete objects, which is not aligned with the observer motion. This contribution studied [120] in detail is not boosted by the Ellis-Baldwin coefficient  $\mathcal{M}$ , and it is too small to make up the difference in observations. In conclusion, the matter density contribution to the intrinsic dipole power becomes quickly negligible at higher redshift, as it samples the matter power spectrum at  $k \simeq 1/\bar{r}_z$  and it averages out with larger width in the redshift distribution. However, it is important to keep in mind that the intrinsic dipole mostly from the matter density fluctuations can be as large as the contribution of the observer motion at  $z \simeq 0.5$ , where various curves cross the gray horizon line  $C_1^{\text{Planck}}$ .

Similar calculations have been performed [14, 21, 102, 120, 121] in the past, regarding the contributions to the dipole power from the matter density fluctuations with various redshift ranges of the galaxy samples.

## VI. DISCUSSION AND SUMMARY

We have critically investigated the origin of the dipole signals from the cosmic microwave background anisotropies (CMB), supernova observations, and galaxy surveys. The observed sources in these large-scale surveys such as CMB photons, supernovae, or galaxies collectively form an effective fluid, in which an intrinsic velocity of the sources can be assigned at the observer position. The dipole signals from these large-scale surveys arise from the relative velocity between the observer velocity and the intrinsic velocity of the sources. While the observer velocity is common in all dipole signals, the intrinsic velocities differ for each large-scale structure probe. However, the contributions to the intrinsic velocities

fall steeply as the effective redshift of the sources increases, and the dominant contribution to the dipole signals is the observer velocity.

This interpretation of the dipole signals, however, depends on our choice of gauge condition, which is implicitly made in the literature to be the conformal Newtonian gauge. In general relativity, only the relative velocity between two motions at the same spacetime position is physically meaningful, not the absolute velocity of one motion, or the relative motion at two different positions. Measurements of the cosmic dipoles are indeed the measurements of the relative velocities between the source and the observer velocities, but the observer velocity in the conformal Newtonian gauge is to a good approximation much larger than the source velocity in the same gauge. Since these relative velocity measurements depend on the observer position, there is no common rest frame in which observers at any spacetime position see no dipoles.

Beside the observer motion, the next-leading contribution to the dipole power arises from the matter density fluctuations in the comoving gauge. As evident in Figure 2, its contribution is dominant, but its effective contribution is greatly reduced in amplitude upon averaging over the redshift distributions of the samples, as shown in Figure 3. In practice, the intrinsic velocity from the matter density fluctuations is negligible for the samples, as long as effective redshift distribution is larger than  $z = 0.5$ . For example, the observed dipole power  $C_1^{\text{obs}}$  from the CatWise survey is larger by a factor 30 than  $C_1$  from the matter density fluctuations, and of course twice larger than the Ellis-Baldwin prediction  $C_1^{\text{EB}}$  from the observer motion measured in the Planck observations [21, 102]. This observational tension detected in many galaxy/quasar samples with various statistical significance [14, 19–23] constitutes a potential challenge to the standard model of cosmology.

In our numerical computation, we have assumed the standard  $\Lambda$ CDM model, but our equations are valid for beyond-the-standard models such as isocurvature models under the assumption that there is no significant anisotropic pressure. Furthermore, we have assumed that the observer moves together with the matter component and only the linear-order contributions were accounted for. Of course, the observer is bound in the Earth, which moves around the Sun and the Galactic center. Such motions are indeed corrected for in the observations, and numerical simulations show that dark matter halos that can host galaxies like ours move as a matter component, or no velocity bias [130]. Nonlinearities in the matter density fluctuations can change the dipole signals, in particular for galaxy surveys (no density contributions in CMB or SN surveys), though the scales  $k \sim 1/\bar{r}_z$  we probe for the dipole measurements are often in the linear regime ( $k \ll 0.1 \text{ hMpc}^{-1}$ ), where the nonlinear boost in the matter density fluctuation is negligible. Unless the effective redshift of the galaxy samples is less than  $z \lesssim 0.5$ , our calculations based on the linear-order perturbation theory remain robust, and the intrinsic velocity contributions are small.

We acknowledge useful discussions with Ruth Durrer, Sebastian von Hausegger, and Subir Sarkar. This work is support

by the Swiss National Science Foundation and a Consolidator Grant of the European Research Council.

## Appendix A: Detailed Calculations

### 1. Notation Convention

Here we present our notation convention used in the text. The metric perturbations around the Robertson-Walker metric are defined in terms of four variables  $\alpha, \beta, \varphi, \gamma$  as

$$\delta g_{00} = -2 a^2 \alpha, \quad \delta g_{0\alpha} = -a^2 \nabla_\alpha \beta, \quad (\text{A1})$$

$$\delta g_{\alpha\beta} = 2 a^2 (\varphi \delta_{\alpha\beta} + \nabla_\alpha \nabla_\beta \gamma), \quad (\text{A2})$$

where we only consider the scalar perturbations. Fluid velocities including the observer motion are described by four velocity vectors  $u^\mu$  subject to the time-like condition  $-1 = u_\mu u^\mu$ , and the four velocity vector is parametrized by

$$u^\mu = \frac{1}{a} (1 - \alpha, -\nabla^\alpha U), \quad (\text{A3})$$

where we introduced the scalar perturbation  $U$  for the spatial velocity component. The indices  $\mu, \nu$  represent the space-time components, while the indices  $\alpha, \beta$  represent the spatial components.

These perturbations are gauge-dependent, or they change their values, depending on our choice of gauge condition. Hence, it is important to ensure that our theoretical description of physical observables is gauge-invariant. We presented in the text our gauge-invariant expressions for the cosmological observables without choosing any gauge conditions, but in general our computation is performed in the conformal Newtonian gauge, in which the spatial gauge is fixed with  $\gamma \equiv 0$  and the temporal gauge is fixed with  $\beta \equiv 0$ , so that the combination  $\chi := a(\beta + \gamma')$  vanishes. Two gravitational potentials  $\psi, \phi$  in the conformal Newtonian gauge correspond to the gauge-invariant Bardeen variables [31]:

$$\psi = \alpha - \frac{1}{a} \chi', \quad \phi = \varphi - H \chi. \quad (\text{A4})$$

The Newtonian gauge velocity corresponds to another gauge-invariant Bardeen variable [31]

$$v^{\text{cN}} = v - \frac{1}{a} \chi, \quad (\text{A5})$$

where we defined a useful combination  $v := U + \beta$ . The matter density fluctuation  $\delta$  in general is gauge-dependent, but the density fluctuation in the rest frame of matter is also gauge-invariant, which corresponds to the comoving-gauge density fluctuation:

$$\delta_v = \delta + 3\mathcal{H}v, \quad (\text{A6})$$

where  $\mathcal{H} = aH$  is the conformal Hubble parameter.

## 2. Observed Galaxy Number Density and Luminosity Distance

The galaxy number density  $n_g(x^\mu)$  at a given position  $x^\mu$  can be split into the background number density  $\bar{n}_g(\eta)$  and the fluctuation  $\delta$  around the mean:  $n_g(x^\mu) = \bar{n}_g(\eta)(1 + \delta)$ . In the simplest model of galaxy formation [40, 131], the galaxy number density fluctuation is related to the matter density fluctuation with a linear bias factor  $b$  in the rest frame of galaxies and matter, which coincides with the comoving gauge ( $v \equiv 0$ ) at the linear order in perturbations. Hence, we obtain the expression for the galaxy number density as

$$n_g(x^\mu) = \bar{n}_g(\eta_v)(1 + b \delta_v), \quad (\text{A7})$$

where the subscript  $v$  indicates that the quantities are evaluated in the comoving gauge. When expressed at the observed redshift  $z$ , instead of a time coordinate  $\eta$ , the galaxy number density becomes

$$n_g = \bar{n}_g(z)(1 + b \delta_v - e_z \delta z_v), \quad (\text{A8})$$

where the distortion  $\delta z$  in the observed redshift at the position  $\eta(\bar{z})$  is defined as

$$1 + z =: (1 + \bar{z})(1 + \delta z), \quad (\text{A9})$$

and the evolution bias factor is defined as

$$e_z := \frac{d \ln \bar{n}_g}{d \ln(1 + z)}. \quad (\text{A10})$$

Note that the redshift  $\bar{z}$  is just an expression for the time coordinate  $\eta$ , and  $e_z = 3$  corresponds to a constant comoving number density such as the matter component. Both quantities  $\delta_v$  and  $\delta z_v$  are gauge invariant:

$$\delta z_v := \delta z + \mathcal{H}v. \quad (\text{A11})$$

Furthermore, the galaxy sample is often selected with a threshold luminosity  $L_t$ , i.e.,  $n_g = n_g(L \geq L_t)$ , where the threshold luminosity at the observed position is defined in terms of the threshold flux  $f_t$  and the background luminosity distance  $\bar{D}_L(z)$  as

$$L_t := 4\pi \bar{D}_L^2(z) f_t. \quad (\text{A12})$$

In the presence of inhomogeneities in the Universe, the luminosity distance  $D_L(z, \hat{n})$  at the observed position fluctuates around the background luminosity distance  $\bar{D}_L(z)$  as

$$D_L(z, \hat{n}) = \bar{D}_L(z)(1 + \delta D). \quad (\text{A13})$$

The (dimensionless) fluctuation  $\delta D$  in the luminosity distance is the same as the fluctuation in the angular diameter distance, and its gauge-invariant expression can be obtained [34, 87–93] by computing the physical area subtended by the observed angle  $d^2 \hat{n}$  at the observed redshift  $z$  as

$$\delta D = \delta z + \frac{\delta r}{\bar{r}_z} - \kappa + \frac{1}{2} (\mathcal{C}_\alpha^\alpha - \mathcal{C}_\parallel), \quad (\text{A14})$$

where  $\delta r$  is the radial distortion,  $\kappa$  is the convergence, and the bracket at the source position is

$$\mathcal{C}_\alpha^\alpha - \mathcal{C}_\parallel = 2\varphi + \Delta\gamma - \partial_\parallel^2 \gamma. \quad (\text{A15})$$

The luminosity distance observation in supernova surveys yields  $D_L(z, \hat{n})$ , including not only the background luminosity distance  $\bar{D}_L(z)$ , but also the fluctuation  $\delta D(z, \hat{n})$ .

Hence, the physical luminosity  $L_p$  set by the threshold flux  $f_t$  at the position of galaxies is different from  $L_t$ :

$$L_p = 4\pi D_L^2(z) f_t = L_t(1 + 2 \delta D), \quad (\text{A16})$$

and the galaxy sample with  $f \geq f_t$  at the observed redshift corresponds to

$$\bar{n}_g(L \geq L_p) = \bar{n}_g(L_t)(1 - t_L \delta D), \quad (\text{A17})$$

where  $\bar{n}_g(L_t) := \bar{n}_g(L \geq L_t)$  for simplicity and we defined the coefficient  $t_L$  evaluated at  $L_t$  as

$$t_L := -2 \frac{d \ln \bar{n}_g(L)}{d \ln L}. \quad (\text{A18})$$

If the luminosity function is approximated as a power-law  $d\bar{n}_g/dL \propto L^{-s}$  at the threshold or the cumulative number density  $\bar{n}_g(L) \propto L^{-s+1}$ , the coefficient  $t_L$  is related to the power-law slope  $s$  as

$$t_L = 2(s-1) =: 5p, \quad p = 0.4(s-1), \quad (\text{A19})$$

where  $p$  is the slope in terms of magnitude  $M = -2.5 \log_{10} L + \text{const}$ , or

$$\log_{10} \bar{n}_g = -2.5p \log_{10} L + \text{const.} = p M + \text{const.} \quad (\text{A20})$$

In the observed galaxy number density, there exists additional contribution  $2 \delta D$  from the volume fluctuation  $\delta V$  described in Eq. (34), such that the total contribution is

$$-t_L \delta D + 2 \delta D \simeq (t_L - 2)\kappa = (2s - 4)\kappa = (5p - 2)\kappa, \quad (\text{A21})$$

and the coefficient of  $\kappa$  is known as the magnification bias factor [114–117], where we used  $\delta D \simeq -\kappa$ . Hence, the source effect  $\delta S$  of the observed galaxy fluctuation is composed of

$$\delta S = b \delta_v - e_z \delta z_v - t_L \delta D. \quad (\text{A22})$$

The observed galaxy fluctuation also arises from the volume effect  $\delta V$ , or the distortion in the physical volume occupied by the observed galaxies, compared to the volume the observer infers, and the volume effect can be obtained [109–113] by following the geodesic path and computing the physical volume subtended by the observed angle  $d^2 \hat{n}$  and the observed redshift  $dz$  as

$$\begin{aligned} \delta V &= 3 \delta z + \delta g + 2 \frac{\delta r}{\bar{r}_z} - 2\kappa + H \frac{d}{dz} \delta r - \alpha + \mathcal{U}_\parallel \\ &= 2 \delta D + \delta z + H \frac{d}{dz} \delta r + \varphi + \mathcal{U}_\parallel + \partial_\parallel^2 \gamma, \end{aligned} \quad (\text{A23})$$

where the fluctuation in the metric determinant is  $\delta g = \alpha + 3\varphi + \Delta\gamma$ . Therefore, the fluctuation in the observed galaxy number density  $n_g^{\text{obs}} = \bar{n}_g(z)(1 + \delta_g)$  is then

$$\delta_g = b \delta_v - e_z \delta z_v - t_L \delta D + \delta V. \quad (\text{A24})$$

The notation convention in [120] corresponds to

$$\begin{aligned} f_{\text{evo}} &\rightarrow 3 - e_z, & 5s &\rightarrow t_L, & (\text{A25}) \\ V_{\text{obs}} &\rightarrow -(\partial_{\parallel} v)_{\bar{o}}, & \Psi &\rightarrow \alpha_{\chi}, & \Phi &\rightarrow -\varphi_{\chi}. \end{aligned}$$

### 3. Scalar Computation

To facilitate the computation, we choose the conformal Newtonian gauge ( $\beta \equiv \gamma \equiv \chi \equiv 0$ ). Furthermore, we only consider *scalar* perturbations, ignoring the vector and tensor perturbation. Under the approximation that there exist negligible anisotropic pressure, two gravitational potentials in the Newtonian gauge are equivalent  $\psi = -\phi$ .

The radial distortion  $\delta r$  of the source, the distortion  $\delta z$  in the observed redshift, and the gravitational lensing convergence  $\kappa$  can be computed in the conformal Newtonian gauge as

$$\delta r = -v_{\bar{o}} - \frac{\delta z}{\mathcal{H}_z} + 2 \int_0^{\bar{r}_z} d\bar{r} \psi + n_{\alpha} \delta x_{\bar{o}}^{\alpha}, \quad (\text{A26})$$

$$\delta z = -\mathcal{H}v_{\bar{o}} - [\partial_{\parallel} v + \psi]_0^z - 2 \int_0^{\bar{r}_z} d\bar{r} \psi', \quad (\text{A27})$$

$$-2\kappa = -2(\partial_{\parallel} v)_{\bar{o}} - \frac{2n_{\alpha} \delta x_{\bar{o}}^{\alpha}}{\bar{r}_z} - 2 \int_0^{\bar{r}_z} d\bar{r} \left( \frac{\bar{r}_z - \bar{r}}{\bar{r}_z \bar{r}} \right) \hat{\nabla}^2 \psi,$$

where all the quantities are in the conformal Newtonian gauge, the observer position  $\bar{x}_{\bar{o}}^{\mu} = (\eta_{\bar{o}}, 0)$  in the background is represented as  $\bar{o}$ , and the conformal time today is

$$\eta_{\bar{o}} = \int_0^{\infty} \frac{dz}{H(z)}. \quad (\text{A28})$$

The derivative term in the volume effect  $\delta V$  can be further manipulated as

$$\begin{aligned} H \frac{d}{dz} \delta r &= -\frac{\mathcal{H}'}{\mathcal{H}^2} \delta z + \frac{1}{\mathcal{H}} \partial_{\parallel}^2 v - \frac{1}{\mathcal{H}} \partial_{\parallel} (-\psi + v') + \frac{\psi'}{\mathcal{H}} + 2\psi \\ &= -\frac{\mathcal{H}'}{\mathcal{H}^2} \delta z + \frac{1}{\mathcal{H}} \partial_{\parallel}^2 v + \partial_{\parallel} v + \frac{\psi'}{\mathcal{H}} + 2\psi, \end{aligned}$$

where in the last equality we used the conservation equation  $v' + \mathcal{H}v = \psi$ .

At the linear order in perturbations, the contributions to the observed galaxy number density fluctuation  $\delta_g(z, \hat{n})$ , the luminosity distance fluctuation  $\delta D(z, \hat{n})$ , or the observed CMB temperature anisotropies  $\Theta_{\gamma}^{\text{obs}}(\hat{n})$  are composed of three distinct types: one at the source position, one at the observer position, and one along the line-of-sight direction, e.g.,

$$\delta_g =: \delta_s + \delta_{\bar{o}} + \delta_{\text{los}}. \quad (\text{A29})$$

The individual terms at the observer position  $\delta_{\bar{o}}$  contribute to the angular monopole and the dipole at the linear order in perturbations (quadrupole as well, if we consider the tensor perturbations). All the terms in  $\delta_s$  and  $\delta_{\text{los}}$  contribute to all angular multipoles, including the monopole and the dipole.

First, we collect all the terms at the observer position:

$$(\delta z)_{\bar{o}} = -\mathcal{H}_0 v_{\bar{o}} + (\partial_{\parallel} v)_{\bar{o}} + \psi_{\bar{o}}, \quad (\text{A30})$$

$$(\delta r)_{\bar{o}} = -\frac{1}{\mathcal{H}_z} (\partial_{\parallel} v + \psi)_{\bar{o}}, \quad (\text{A31})$$

$$-2(\kappa)_{\bar{o}} = -2(\partial_{\parallel} v)_{\bar{o}}. \quad (\text{A32})$$

With these expressions, we obtain

$$(\Theta_{\gamma}^{\text{obs}})_{\bar{o}} = \mathcal{H}_0 v_{\bar{o}} - \psi_{\bar{o}} - (\partial_{\parallel} v)_{\bar{o}}, \quad (\text{A33})$$

$$(\delta D)_{\bar{o}} = -\mathcal{H}_0 v_{\bar{o}} \left( 1 - \frac{1}{\mathcal{H}_z \bar{r}_z} + \frac{1}{\mathcal{H}_0 \bar{r}_z} \right) \quad (\text{A34})$$

$$\begin{aligned} &+ \psi_{\bar{o}} \left( 1 - \frac{1}{\mathcal{H}_z \bar{r}_z} \right) - \frac{(\partial_{\parallel} v)_{\bar{o}}}{\mathcal{H}_z \bar{r}_z}, \\ (\delta_g)_{\bar{o}} &= \mathcal{H}v_{\bar{o}} \left[ h_z - 3 - \frac{2}{\mathcal{H}_0 \bar{r}_z} + t_L \left( 1 - \frac{1}{\mathcal{H}_z \bar{r}_z} + \frac{1}{\mathcal{H}_0 \bar{r}_z} \right) \right] \\ &- (\partial_{\parallel} v)_{\bar{o}} \left( h_z - 1 - \frac{t_L}{\mathcal{H}_z \bar{r}_z} \right) \\ &- \psi_{\bar{o}} \left[ h_z - 3 + t_L \left( 1 - \frac{1}{\mathcal{H}_z \bar{r}_z} \right) \right], \quad (\text{A35}) \end{aligned}$$

where we defined the time-dependent coefficient [119]

$$h(z) := e_z + \frac{2}{\mathcal{H}_z \bar{r}_z} + \frac{\mathcal{H}'_z}{\mathcal{H}_z^2}. \quad (\text{A36})$$

Note that the full expression for the observed CMB temperature anisotropies is presented in Eq. (5).

Last, the line-of-sight contributions  $\delta_{\text{los}}$  and the contributions  $\delta_s$  at the source position can be readily read off from the equations above, and the final expressions are

$$(\Theta_\gamma^{\text{obs}})_{\text{los}} = \int_0^{\bar{r}_*} d\bar{r} \, 2\psi', \quad (\Theta_\gamma^{\text{obs}})_s = \Theta_* + \psi + (\partial_\parallel v), \quad (\text{A37})$$

$$(\delta D)_{\text{los}} = -2 \left(1 - \frac{1}{\mathcal{H}_z \bar{r}_z}\right) \int_0^{\bar{r}_z} d\bar{r} \, \psi' + \frac{2}{\bar{r}_z} \int_0^{\bar{r}_z} d\bar{r} \, \psi - \int_0^{\bar{r}_z} d\bar{r} \left( \frac{\bar{r}_z - \bar{r}}{\bar{r}_z \bar{r}} \right) \hat{\nabla}^2 \psi, \quad (\text{A38})$$

$$(\delta D)_s = -\partial_\parallel v \left(1 - \frac{1}{\mathcal{H}_z \bar{r}_z}\right) - \psi \left(2 - \frac{1}{\mathcal{H}_z \bar{r}_z}\right), \quad (\text{A39})$$

$$(\delta g)_{\text{los}} = \int_0^{\bar{r}_z} d\bar{r} \left\{ \frac{4-2t_L}{\bar{r}_z} \psi + \left[ 2(h_z-3) + 2t_L \left(1 - \frac{1}{\mathcal{H}_z \bar{r}_z}\right) \right] \psi' + (t_L-2) \left( \frac{\bar{r}_z - \bar{r}}{\bar{r}_z \bar{r}} \right) \hat{\nabla}^2 \psi \right\}, \quad (\text{A40})$$

$$(\delta g)_s = b \delta_v + \frac{1}{\mathcal{H}_z} \partial_\parallel^2 v + \left[ h_z - 3 + t_L \left(1 - \frac{1}{\mathcal{H}_z \bar{r}_z}\right) \right] \partial_\parallel v + \left[ h_z - 4 + t_L \left(2 - \frac{1}{\mathcal{H}_z \bar{r}_z}\right) \right] \psi - e_z \mathcal{H}_z v + \frac{\psi'}{\mathcal{H}_z}. \quad (\text{A41})$$

#### 4. Angular Decomposition and Transfer Functions

With three distinct types of contributions in Eq. (A29), each type can be Fourier decomposed as

$$\delta_s = \int \frac{d^3 k}{(2\pi)^3} e^{i\mathbf{k} \cdot \mathbf{x}_s} \delta_s(k, \bar{r}_z), \quad (\text{A42})$$

$$\delta_{\bar{o}} = \int \frac{d^3 k}{(2\pi)^3} \delta_{\bar{o}}(k, 0), \quad (\text{A43})$$

$$\delta_{\text{los}} = \int \frac{d^3 k}{(2\pi)^3} \int_0^{\bar{r}_z} d\bar{r} e^{i\mathbf{k} \cdot \mathbf{x}_{\bar{r}}} \delta_{\text{los}}(k, \bar{r}), \quad (\text{A44})$$

where the position vector  $\mathbf{x} = \bar{r}\hat{\mathbf{n}}$  and the contributions  $\delta_{\bar{o}}$  at the observer position are the usual Fourier transformation evaluated at  $\bar{o}$  (hence the exponential factor is unity). In each type, there exist numerous perturbation contributions, and we

define the transfer function  $\mathcal{T}_{\delta p}$  to describe these perturbations, e.g.,

$$\delta p(\mathbf{k}, \eta) =: \mathcal{T}_{\delta p}(k, \eta) \mathcal{R}(\mathbf{k}), \quad (\text{A45})$$

in terms of the comoving-gauge curvature perturbation  $\mathcal{R}(\mathbf{k})$  at the initial time. Note that in expressing the transfer function  $\mathcal{T}_{\delta p}(k, \eta)$  we have interchangeably used the redshift  $z$  or the comoving distance  $\bar{r}$  for the time coordinate  $\eta$  throughout the manuscript. As the observed galaxy fluctuation  $\delta_g$  or the luminosity distance fluctuation  $\delta D$  is angular decomposed in terms of spherical harmonics  $Y_{lm}(\hat{\mathbf{n}})$  as

$$\delta_g(z, \hat{\mathbf{n}}) = \sum_{lm} a_{lm}(z) Y_{lm}(\hat{\mathbf{n}}), \quad (\text{A46})$$

the angular multipoles can be obtained as

$$a_{lm}(z) = \int d^2 \hat{\mathbf{n}} Y_{lm}^*(\hat{\mathbf{n}}) \delta_g(z, \hat{\mathbf{n}}) = 4\pi i^l \int \frac{dk k^2}{2\pi^2} \left[ \underbrace{\mathcal{T}_{\delta p}(k, z) j_l(k\bar{r}_z) + \dots}_{=: \mathcal{T}_l(k, z)} \right] \int \frac{d\Omega_k}{4\pi} Y_{lm}^*(\hat{\mathbf{k}}) \mathcal{R}(\mathbf{k}), \quad (\text{A47})$$

where we used the plane-wave expansion

$$e^{i\mathbf{k} \cdot \mathbf{x}} = 4\pi \sum_{lm} i^l j_l(kr) Y_{lm}^*(\hat{\mathbf{k}}) Y_{lm}(\hat{\mathbf{n}}), \quad (\text{A48})$$

$\mathcal{T}_{\delta p}$  is the transfer function for individual perturbation contributions, and we defined the full angular multipole transfer function  $\mathcal{T}_l(k, z)$  inside the square bracket. Mind that the transfer function is real. Given the ensemble average in the initial conditions

$$\begin{aligned} \langle \mathcal{R}(\mathbf{k}_1) \mathcal{R}^*(\mathbf{k}_2) \rangle &= (2\pi)^3 \delta^D(\mathbf{k}_1 - \mathbf{k}_2) P_{\mathcal{R}}(k_1) \\ &= \frac{(2\pi)^3}{k_1^2} P_{\mathcal{R}}(k_1) \delta^D(k_1 - k_2) \delta^D(\Omega_{k_1} - \Omega_{k_2}), \end{aligned} \quad (\text{A49})$$

the angular power spectrum can be obtained as

$$\begin{aligned} \langle a_{lm}(z_1) a_{l'm'}^*(z_2) \rangle &= \delta_{ll'} \delta_{mm'} C_l(z_1, z_2) \\ &= \delta_{ll'} \delta_{mm'} \times 4\pi \int d \ln k \Delta_{\mathcal{R}}^2(k) \mathcal{T}_l(k, z_1) \mathcal{T}_l(k, z_2). \end{aligned} \quad (\text{A50})$$

First, we compute the transfer function  $\mathcal{T}_l(k, z)$  for the contributions at the source position. For the various contributions at the source position in Eqs. (A37), (A39), and (A41), the angular momentum dependence arises primarily from the exponential in the plane wave expansion in Eq. (A48). However, the contributions with additional dependence on  $\hat{\mathbf{n}}$  have an intrinsic angular momentum, which needs to be added to the orbital angular momentum from the plane wave expansion.

The contributions without additional angular dependence take the form  $C_i(z) \delta p_i(z, \hat{\mathbf{n}})$  in Eqs. (A39) and (A41), and their contributions to the dipole transfer function can be read off by using Eq. (A47) as

$$\mathcal{T}_1(k, z) \ni C_i(z) \mathcal{T}_{\delta p_i}(k, z) j_1(k\bar{r}_z), \quad (\text{A51})$$

where the redshift-dependent coefficients for the observed

galaxy fluctuation are

$$\begin{aligned} C_{\delta v} &:= b, & C_v &:= -e_z \mathcal{H}_z, & C_{\psi'} &:= \frac{1}{\mathcal{H}_z}, \\ C_\psi &:= h_z - 4 + t_L \left( 2 - \frac{1}{\mathcal{H}_z \bar{r}_z} \right), & & & & \end{aligned} \quad (\text{A52})$$

that for the luminosity distance fluctuation is

$$C_{\psi}^{\delta D} := -2 + \frac{1}{\mathcal{H}_z \bar{r}_z}, \quad (\text{A53})$$

and those for the observed CMB temperature anisotropies are

$$C_{\Theta}^{\gamma} := 1, \quad C_{\psi}^{\gamma} := 1. \quad (\text{A54})$$

We put the superscript  $\delta D$  or  $\gamma$  to contrast the difference in the quantities for the luminosity distance fluctuation and the CMB temperature anisotropies, compared to the quantities for the observed galaxy fluctuation.

The transfer function for the line-of-sight peculiar velocity  $(\partial_{\parallel} v)$  at the source position can be obtained by acting the line-of-sight derivative for the transfer function of the  $v$ -contribution shown in Eq. (A47). The derivative operator  $\partial_{\parallel}$  acts on the spherical Bessel function  $j_l(k\bar{r}_z)$  to yield

$$\mathcal{T}_1(k, z) \ni C_{\partial_{\parallel} v}(z) k \mathcal{T}_v(k, z) j_1'(k\bar{r}_z), \quad (\text{A55})$$

where the redshift-dependent coefficients are

$$C_{\partial_{\parallel} v} := h_z - 3 + t_L \left( 1 - \frac{1}{\mathcal{H}_z \bar{r}_z} \right), \quad (\text{A56})$$

$$C_{\partial_{\parallel} v}^{\delta D} := -1 + \frac{1}{\mathcal{H}_z \bar{r}_z}, \quad C_{\partial_{\parallel} v}^{\gamma} := 1. \quad (\text{A57})$$

With the spherical Bessel function identity

$$j_l'(x) = \frac{l}{2l+1} j_{l-1}(x) - \frac{l+1}{2l+1} j_{l+1}(x), \quad (\text{A58})$$

it is clear that the derivative operator brings in additional angular momentum to the orbital angular momentum of the velocity contribution at the source position.

In the same way, two derivatives  $(\partial_{\parallel}^2 v)$  of the line-of-sight peculiar motion at the source position yield the transfer function

$$\mathcal{T}_1(k, z) \ni \frac{k^2}{\mathcal{H}_z} \mathcal{T}_v(k, z) j_1''(k\bar{r}_z), \quad (\text{A59})$$

which arises from the redshift-space distortion [4]. The luminosity distance fluctuation  $\delta D$  or the observed CMB temperature anisotropies has no such contribution. Again, the angular momentum addition can be obtained by using

$$\begin{aligned} j_l''(x) &= \frac{l(l-1)}{(2l+1)(2l-1)} j_{l-2}(x) - \frac{2l^2+2l-1}{(2l-1)(2l+3)} j_l(x) \\ &\quad + \frac{(l+1)(l+2)}{(2l+1)(2l+3)} j_{l+2}(x). \end{aligned}$$

Second, we consider the line-of-sight contributions to the angular multipole transfer function. These contributions include three possibilities: the line-of-sight integration of  $\psi$ , the line-of-sight integration of  $\psi'$ , or the lensing contribution, which we parametrize as

$$\int_0^{\bar{r}_z} d\bar{r} \left[ L_{\psi}(z) \psi + L_{\psi'}(z) \psi' + (t_L - 2) \left( \frac{\bar{r}_z - \bar{r}}{\bar{r}_z \bar{r}} \right) \hat{\nabla}^2 \psi \right]. \quad (\text{A60})$$

Each component at one point along the line-of-sight direction can be decomposed exactly in the same way as for the contributions at the source position, except the lensing contribution, where the angular Laplacian operator  $\hat{\nabla}^2$  acts on the spherical harmonics to yield

$$\hat{\nabla}^2 Y_{lm}(\hat{n}) = -l(l+1) Y_{lm}(\hat{n}). \quad (\text{A61})$$

Altogether, the angular multipole transfer function from the line-of-sight contributions in Eqs. (A37), (A38), and (A40) is

$$\mathcal{T}_l(k, z) \ni \int_0^{\bar{r}_z} d\bar{r} \left[ L_{\psi}(z) \mathcal{T}_{\psi}(k, \bar{r}) + L_{\psi'}(z) \mathcal{T}_{\psi'}(k, \bar{r}) - l(l+1)(t_L - 2) \left( \frac{\bar{r}_z - \bar{r}}{\bar{r}_z \bar{r}} \right) \mathcal{T}_{\psi}(k, \bar{r}) \right] j_l(k\bar{r}), \quad (\text{A62})$$

where the redshift-dependent coefficients are

$$L_{\psi} = \frac{4 - 2t_L}{\bar{r}_z}, \quad (\text{A63})$$

$$L_{\psi'} = 2(h_z - 3) + 2t_L \left( 1 - \frac{1}{\mathcal{H}_z \bar{r}_z} \right), \quad (\text{A64})$$

for the observed galaxy fluctuation, and

$$L_{\psi}^{\delta D} = \frac{2}{\bar{r}_z}, \quad L_{\psi'}^{\delta D} = -2 \left( 1 - \frac{1}{\mathcal{H}_z \bar{r}_z} \right), \quad (\text{A65})$$

for the luminosity distance fluctuation, and  $L_{\psi'}^{\gamma} = 2$  for the observed CMB temperature anisotropies.

Next, we compute the transfer functions from the contributions at the observer position. Among all the contributions at the observer position in Eqs. (A33), (A34), and (A35), only the peculiar motion  $(\partial_{\parallel} v)_{\circ}$  of the observer possesses the directional dependence  $\hat{n}$ , contributing to the dipole transfer function, while the remaining terms at the observer position contribute to the monopole transfer function. This contribution to the dipole transfer function can be written in Fourier space as

$$O_{\partial_{\parallel} v}(z) (\partial_{\parallel} v)_{\circ} = \int \frac{d^3 k}{(2\pi)^3} \left[ O_{\partial_{\parallel} v}(z) (i\mathbf{k} \cdot \mathbf{n}) \mathcal{T}_v(k, \eta_{\circ}) \right] \mathcal{R}(\mathbf{k}), \quad (\text{A66})$$

where the derivative operator acted on the Fourier mode before getting evaluated at the observer position. The redshift-dependent coefficients for the observed galaxy fluctuation and the luminosity distance are

$$O_{\partial_{\parallel}v} := 1 - h_z + \frac{t_L}{\mathcal{H}_z \bar{r}_z}, \quad (\text{A67})$$

$$O_{\partial_{\parallel}v}^{\delta D} := -\frac{1}{\mathcal{H}_z \bar{r}_z}, \quad O_{\partial_{\parallel}v}^{\gamma} = -1. \quad (\text{A68})$$

Expressing the unit directional vectors  $\hat{n}$  and  $\hat{k}$  in terms of spherical harmonics,

$$\hat{n} = (\sin \theta \cos \phi, \sin \theta \sin \phi, \cos \theta) = \sqrt{\frac{4\pi}{3}} \left( \frac{Y_{1,-1}(\hat{n}) - Y_{1,1}(\hat{n})}{\sqrt{2}}, i \frac{Y_{1,-1}(\hat{n}) + Y_{1,1}(\hat{n})}{\sqrt{2}}, Y_{10}(\hat{n}) \right), \quad (\text{A69})$$

the inner product of two directional vectors is

$$\hat{k} \cdot \hat{n} = \frac{4\pi}{3} \left[ Y_{1,1}(\hat{n}) Y_{1,1}^*(\hat{k}) + Y_{1,-1}(\hat{n}) Y_{1,-1}^*(\hat{k}) + Y_{10}(\hat{n}) Y_{10}(\hat{k}) \right], \quad (\text{A70})$$

where we used  $Y_{l,-m} = (-1)^m Y_{lm}^*$  and  $Y_{11} = -Y_{1,-1}^*$  to simplify the expression. Hence we derive the angular dipole coefficient

$$a_{1m} = 4\pi i \int \frac{dk k^2}{2\pi^2} \left\{ \left[ O_{\partial_{\parallel}v}(z) \frac{k}{3} \mathcal{T}_v(k, \eta_{\bar{0}}) \right] (\delta_{m0} + \delta_{m,1} + \delta_{m,-1}) \right\} \int \frac{d\Omega_k}{4\pi} Y_{1m}^*(\hat{k}) \mathcal{R}(\mathbf{k}), \quad (\text{A71})$$

where the dipole transfer function includes the quantities in the curly bracket. Though the dipole transfer function from the peculiar motion at the observer motion depends on the value of  $m$ , the dipole power spectrum is averaged over  $m$  as

$$C_1 = \langle |a_{1m}|^2 \rangle = \frac{1}{3} \sum_m \langle |a_{1m}|^2 \rangle, \quad (\text{A72})$$

and each  $m$ -mode contributes equally to the dipole power, such that the  $m$ -dependence can be ignored and the dipole

transfer function is simply the quantity in the square bracket:

$$\mathcal{T}_1(k, z) \ni O_{\partial_{\parallel}v}(z) \frac{k}{3} \mathcal{T}_v(k, \eta_{\bar{0}}). \quad (\text{A73})$$

## 5. Dipole Transfer Functions

Collecting all the contributions from the source position, the observer position, and the line-of-sight direction, we obtain the total angular dipole transfer function for the observed galaxy fluctuation:

$$\begin{aligned} \mathcal{T}_1(k, z) &:= O_{\partial_{\parallel}v}(z) \frac{k}{3} \mathcal{T}_v(k, \eta_{\bar{0}}) + \int_0^{\bar{r}_z} d\bar{r} \left[ L_{\psi}(z) \mathcal{T}_{\psi}(k, \bar{r}) + L_{\psi'}(z) \mathcal{T}_{\psi'}(k, \bar{r}) - 2(t_L - 2) \left( \frac{\bar{r}_z - \bar{r}}{\bar{r}_z \bar{r}} \right) \mathcal{T}_{\psi}(k, \bar{r}) \right] j_1(k\bar{r}) \\ &+ \left[ C_{\delta}(z) \mathcal{T}_{\delta}(k, \bar{r}_z) + C_v(z) \mathcal{T}_v(k, \bar{r}_z) + C_{\psi}(z) \mathcal{T}_{\psi}(k, \bar{r}_z) + C_{\psi'}(z) \mathcal{T}_{\psi'}(k, \bar{r}_z) \right] j_1(k\bar{r}_z) \\ &+ C_{\partial_{\parallel}v}(z) k \mathcal{T}_v(k, \bar{r}_z) j_1'(k\bar{r}_z) + \frac{k^2}{\mathcal{H}_z} \mathcal{T}_v(k, \bar{r}_z) j_1''(k\bar{r}_z), \end{aligned} \quad (\text{A74})$$

the total dipole transfer function for the luminosity distance

$$\begin{aligned} \mathcal{T}_1^{\delta D}(k, z) &:= O_{\partial_{\parallel}v}^{\delta D}(z) \frac{k}{3} \mathcal{T}_v(k, \eta_{\bar{0}}) + \int_0^{\bar{r}_z} d\bar{r} \left[ L_{\psi}^{\delta D}(z) \mathcal{T}_{\psi}(k, \bar{r}) + L_{\psi'}^{\delta D}(z) \mathcal{T}_{\psi'}(k, \bar{r}) + 2 \left( \frac{\bar{r}_z - \bar{r}}{\bar{r}_z \bar{r}} \right) \mathcal{T}_{\psi}(k, \bar{r}) \right] j_1(k\bar{r}) \\ &+ C_{\psi}^{\delta D}(z) \mathcal{T}_{\psi}(k, \bar{r}_z) j_1(k\bar{r}_z) + C_{\partial_{\parallel}v}^{\delta D}(z) k \mathcal{T}_v(k, \bar{r}_z) j_1'(k\bar{r}_z), \end{aligned} \quad (\text{A75})$$

and the total dipole transfer function for the observed CMB temperature anisotropies

$$\mathcal{T}_1^{\gamma}(k) := \left[ \mathcal{T}_{\Theta}(k, \eta_{\star}) + \mathcal{T}_{\psi}(k, \eta_{\star}) \right] j_1(k\bar{r}_{\star}) + k \mathcal{T}_v(k, \eta_{\star}) j_1'(k\bar{r}_{\star}) - \frac{1}{3} k \mathcal{T}_v(k, \eta_{\bar{0}}) + \int_0^{\bar{r}_{\star}} d\bar{r} 2 \mathcal{T}_{\psi'}(k, \bar{r}) j_1(k\bar{r}). \quad (\text{A76})$$

The redshift-dependent coefficients for the observed galaxy fluctuation are (put together here again for convenience)

$$O_{\partial_{\parallel}v} := 1 - h_z + \frac{t_L}{\mathcal{H}_z \bar{r}_z}, \quad L_{\psi} = \frac{4 - 2t_L}{\bar{r}_z}, \quad L_{\psi'} = 2(h_z - 3) + 2t_L \left(1 - \frac{1}{\mathcal{H}_z \bar{r}_z}\right), \quad (\text{A77})$$

$$C_{\delta} := b, \quad C_v := -e_z \mathcal{H}_z, \quad C_{\psi} := h_z - 4 + t_L \left(2 - \frac{1}{\mathcal{H}_z \bar{r}_z}\right), \quad (\text{A78})$$

$$C_{\psi'} := \frac{1}{\mathcal{H}_z}, \quad C_{\partial_{\parallel}v} := h_z - 3 + t_L \left(1 - \frac{1}{\mathcal{H}_z \bar{r}_z}\right), \quad h_z = e_z + \frac{2}{\mathcal{H}_z \bar{r}_z} + \frac{\mathcal{H}'_z}{\mathcal{H}_z^2}, \quad (\text{A79})$$

and the redshift-dependent coefficients for the luminosity distance fluctuation are

$$O_{\partial_{\parallel}v}^{\delta D} := -\frac{1}{\mathcal{H}_z \bar{r}_z}, \quad L_{\psi}^{\delta D} := \frac{2}{\bar{r}_z}, \quad L_{\psi'}^{\delta D} := -2 \left(1 - \frac{1}{\mathcal{H}_z \bar{r}_z}\right), \quad (\text{A80})$$

$$C_{\psi}^{\delta D} := -2 + \frac{1}{\mathcal{H}_z \bar{r}_z}, \quad C_{\partial_{\parallel}v}^{\delta D} := -1 + \frac{1}{\mathcal{H}_z \bar{r}_z}. \quad (\text{A81})$$

## Appendix B: Shot Noises

In the text we have presented the contributions of cosmological fluctuations to the dipole power in large-scale structure surveys, but the dipole measurements from large-scale structure surveys inevitably involve measurement noises from various sources such as the detector noise, the telescope re-

sponse function, the survey window function, and so on. Here we consider the shot-noise contribution to the dipole power due to the discreteness of the sources.

The angular number density of galaxies in Eq. (41) can be angular decomposed as  $\Sigma_g^{\text{obs}}(\hat{\mathbf{n}}) = \sum A_{lm} Y_{lm}(\hat{\mathbf{n}})$  and its power can be computed as

$$\langle A_{lm} A_{l'm'}^* \rangle = \int d\Omega_1 Y_{lm}^*(\hat{\mathbf{n}}_1) \int d\Omega_2 Y_{l'm'}(\hat{\mathbf{n}}_2) \int dz_1 \left( \frac{d\bar{V}}{dz d\Omega} \right)_1 \int dz_2 \left( \frac{d\bar{V}}{dz d\Omega} \right)_2 \left[ \bar{n}_1 \bar{n}_2 (1 + \xi_g^{\text{obs}}) + \bar{n}_1 \delta^D(\mathbf{x}_1 - \mathbf{x}_2) \right], \quad (\text{B1})$$

where the subscript 1 and 2 represent the corresponding three-dimensional positions  $\mathbf{x}$  in terms of the observed redshift  $z$  and angle  $\hat{\mathbf{n}}$  and  $\delta^D(\mathbf{x})$  is the Dirac delta function. The first term in the square bracket is the background contribution and the second term is the perturbation contribution or the two-point correlation function, computed in the main text. The last term is the shot-noise contribution arising from the discreteness of individual galaxies in surveys. In the absence of other non-Gaussian systematic errors, the total angular power spectrum including noises is diagonal:

$$C_l^{\text{LSS,tot}} := \langle |A_{lm}|^2 \rangle = 4\pi \bar{\Sigma}_g^2 \delta_{l0} + \bar{\Sigma}_g^2 \left( C_l^{\text{LSS}} + \frac{1}{\bar{\Sigma}_g} \right), \quad (\text{B2})$$

where the expression is valid for  $l \geq 0$  and  $C_{l=0}^{\text{LSS}} \neq 0$  (see [60, 68, 132] for discussion of the monopole fluctuations). Since the background contributes only to the monopole power, we can split the observed angular number density  $\Sigma_g^{\text{obs}}(\hat{\mathbf{n}}) = \bar{\Sigma}_g + \delta\Sigma_g(\hat{\mathbf{n}})$  and angular decompose as

$$\frac{\delta\Sigma_g(\hat{\mathbf{n}})}{\bar{\Sigma}_g} = \sum_{lm} a_{lm} Y_{lm}(\hat{\mathbf{n}}). \quad (\text{B3})$$

The cosmological dipole power  $C_{l=1}^{\text{LSS}} = \langle |a_{1m}|^2 \rangle$  computed in the main text is defined without  $\bar{\Sigma}_g^2$  in the angular power

spectrum  $C_{l=1}^{\text{LSS,tot}}$ , and the shot-noise contribution to be compared to  $C_1^{\text{LSS}}$  is  $C_1^{\text{shot}} = 1/\bar{\Sigma}_g$ , which is the same for all angular multipoles ( $l \geq 0$ ).

Galaxy surveys measure the three-dimensional galaxy number density  $n_g^{\text{obs}}(z, \hat{\mathbf{n}})$ , and it can be angular decomposed as  $n_g^{\text{obs}}(z, \hat{\mathbf{n}}) = \sum A_{lm}(z) Y_{lm}(\hat{\mathbf{n}})$  to measure the angular power spectrum  $C_l(z)$  as a function of redshift (see, e.g., Figure 2). The angular power spectrum in this case can be readily computed by using Eq. (B1) without the integration over the redshift as

$$C_l^{\text{LSS,tot}} = 4\pi \bar{n}_1 \bar{n}_2 \delta_{l0} + \bar{n}_1 \bar{n}_2 \left[ C_l^{\text{LSS}} + \frac{1}{\bar{n}_1} \frac{1}{a^3 \bar{r}_1^2} \delta^D(\bar{r}_1 - \bar{r}_2) \right]. \quad (\text{B4})$$

Mind that the dimension of the galaxy number density is the inverse of physical volume and the quantities in the square bracket is dimensionless. The presence of the Dirac delta function makes the shot-noise contribution infinite, and the method of using  $n_g^{\text{obs}}$  for the angular power spectrum is useful only in theoretical understanding. Of course, the redshift range  $\Delta z$  for computing  $n_g^{\text{obs}}$  in practice is never infinitesimally small, and hence the shot-noise is not infinite either. Nevertheless, the shot-noise contribution in this case is still very large as  $\bar{\Sigma}_g \propto \Delta z$ .

For CMB power spectra, while the width of the last scatter-

ing surface is relatively narrow  $\Delta z$ , the number of CMB photons obtained over the mission duration is sufficiently large

enough to make the shot noise contribution negligible, compared to the detector noise and the cosmic variance contributions to the power spectrum.

- 
- [1] M. Tegmark et al., Phys. Rev. D **74**, 123507 (2006), arXiv:astro-ph/0608632.
  - [2] É. Aubourg, S. Bailey, J. E. Bautista, F. Beutler, et al., Phys. Rev. D **92**, 123516 (2015), 1411.1074.
  - [3] DESI Collaboration, A. G. Adame, J. Aguilar, S. Ahlen, S. Alam, D. M. Alexander, M. Alvarez, O. Alves, A. Anand, U. Andrade, et al., arXiv e-prints arXiv:2404.03002 (2024), 2404.03002.
  - [4] N. Kaiser, Mon. Not. R. Astron. Soc. **227**, 1 (1987).
  - [5] G. F. R. Ellis and J. E. Baldwin, Mon. Not. R. Astron. Soc. **206**, 377 (1984).
  - [6] A. Kogut, C. Lineweaver, G. F. Smoot, C. L. Bennett, A. Banday, N. W. Boggess, E. S. Cheng, G. de Amici, D. J. Fixsen, G. Hinshaw, et al., Astrophys. J. **419**, 1 (1993), astro-ph/9312056.
  - [7] G. Hinshaw, J. L. Weiland, R. S. Hill, N. Odegard, D. Larson, C. L. Bennett, J. Dunkley, B. Gold, M. R. Greason, N. Jarosik, et al., Astrophys. J. Suppl. Ser. **180**, 225 (2009), 0803.0732.
  - [8] Planck Collaboration, N. Aghanim, C. Armitage-Caplan, M. Arnaud, Ashdown, et al., Astron. Astrophys. **571**, A27 (2014), 1303.5087.
  - [9] Planck Collaboration, N. Aghanim, Y. Akrami, F. Arroja, M. Ashdown, J. Aumont, C. Baccigalupi, M. Ballardini, A. J. Banday, R. B. Barreiro, et al., arXiv e-prints (2018), 1807.06205.
  - [10] D. G. York, J. Adelman, J. Anderson, John E., S. F. Anderson, J. Annis, N. A. Bahcall, J. A. Bakken, R. Barkhouser, S. Bastian, E. Berman, et al., Astron. J. **120**, 1579 (2000), arXiv:astro-ph/0006396.
  - [11] M. Colless, G. Dalton, S. Maddox, W. Sutherland, P. Norberg, S. Cole, J. Bland-Hawthorn, T. Bridges, R. Cannon, C. Collins, et al., Mon. Not. R. Astron. Soc. **328**, 1039 (2001), arXiv:astro-ph/0106498.
  - [12] C. Blake and J. Wall, Nature (London) **416**, 150 (2002), astro-ph/0203385.
  - [13] A. K. Singal, Astrophys. J. Lett. **742**, L23 (2011), 1110.6260.
  - [14] C. Gibelyou and D. Huterer, Mon. Not. R. Astron. Soc. **427**, 1994 (2012), 1205.6476.
  - [15] M. Rubart and D. J. Schwarz, Astron. Astrophys. **555**, A117 (2013), 1301.5559.
  - [16] P. Tiwari, R. Kothari, A. Naskar, S. Nadkarni-Ghosh, and P. Jain, Astroparticle Physics **61**, 1 (2015), 1307.1947.
  - [17] P. Tiwari and A. Nusser, J. Cosmol. Astropart. Phys. **2016**, 062 (2016), 1509.02532.
  - [18] J. J. Condon, W. D. Cotton, E. W. Greisen, Q. F. Yin, R. A. Perley, G. B. Taylor, and J. J. Broderick, Astron. J. **115**, 1693 (1998).
  - [19] C. A. P. Bengaly, R. Maartens, and M. G. Santos, J. Cosmol. Astropart. Phys. **2018**, 031 (2018), 1710.08804.
  - [20] A. K. Singal, Mon. Not. R. Astron. Soc. **488**, L104 (2019), 1405.4796.
  - [21] N. J. Secrest, S. von Hausegger, M. Rameez, R. Mohayaee, S. Sarkar, and J. Colin, Astrophys. J. Lett. **908**, L51 (2021), 2009.14826.
  - [22] P. Tiwari, D. J. Schwarz, G.-B. Zhao, R. Durrer, M. Kunz, and H. Padmanabhan, Astrophys. J. **975**, 279 (2024), 2409.09946.
  - [23] A. K. Singal, Mon. Not. R. Astron. Soc. **532**, L1 (2024), 2403.16581.
  - [24] N. Secrest, S. von Hausegger, M. Rameez, R. Mohayaee, and S. Sarkar, Nature Reviews Physics **7**, 68 (2025), 2501.06450.
  - [25] E. L. Wright, P. R. M. Eisenhardt, A. K. Mainzer, M. E. Ressler, R. M. Cutri, T. Jarrett, J. D. Kirkpatrick, D. Padgett, R. S. McMillan, M. Skrutskie, et al., Astron. J. **140**, 1868 (2010), 1008.0031.
  - [26] P. J. E. Peebles, Philosophical Transactions of the Royal Society of London Series A **383**, 20240021 (2025), 2405.18307.
  - [27] A. Lewis, A. Challinor, and A. Lasenby, Astrophys. J. **538**, 473 (2000), arXiv:astro-ph/9911177.
  - [28] D. Blas, J. Lesgourgues, and T. Tram, J. Cosmol. Astropart. Phys. **7**, 034 (2011), 1104.2933.
  - [29] G. F. R. Ellis and W. Stoeger, Class. Quant. Grav. **4**, 1697 (1987).
  - [30] G. F. R. Ellis and M. Bruni, Phys. Rev. D **40**, 1804 (1989).
  - [31] J. M. Bardeen, Phys. Rev. D **22**, 1882 (1980).
  - [32] H. Kodama and M. Sasaki, Progress of Theoretical Physics Supplement **78**, 1 (1984).
  - [33] V. F. Mukhanov, H. A. Feldman, and R. H. Brandenberger, Phys. Rep. **215**, 203 (1992).
  - [34] C. Bonvin, R. Durrer, and M. Kunz, Phys. Rev. Lett. **96**, 191302 (2006), astro-ph/0603240.
  - [35] M. Yoon, D. Huterer, C. Gibelyou, A. Kovács, and I. Szapudi, Mon. Not. R. Astron. Soc. **445**, L60 (2014), 1406.1187.
  - [36] T. M. Siewert, M. Schmidt-Rubart, and D. J. Schwarz, Astron. Astrophys. **653**, A9 (2021), 2010.08366.
  - [37] U. Seljak and M. Zaldarriaga, Astrophys. J. **469**, 437 (1996), astro-ph/9603033.
  - [38] R. Arnowitt, S. Deser, and C. W. Misner, in *Gravitation: An Introduction to Current Research*, vol. 40 (Wiley, New York, 1962), arXiv:0405109.
  - [39] J. Yoo, Phys. Rev. D **90**, 123507 (2014), 1408.5137.
  - [40] N. Kaiser, Astrophys. J. Lett. **284**, L9 (1984).
  - [41] S. Yasini and E. Pierpaoli, Phys. Rev. Lett. **119**, 221102 (2017), 1610.00015.
  - [42] R. Watkins, H. A. Feldman, and M. J. Hudson, Mon. Not. R. Astron. Soc. **392**, 743 (2009), 0809.4041.
  - [43] A. Kashlinsky, F. Atrio-Barandela, D. Kocevski, and H. Ebeling, Astrophys. J. Lett. **686**, L49 (2008), 0809.3734.
  - [44] H. A. Feldman, R. Watkins, and M. J. Hudson, Mon. Not. R. Astron. Soc. **407**, 2328 (2010), 0911.5516.
  - [45] S. J. Turnbull, M. J. Hudson, H. A. Feldman, M. Hicken, R. P. Kirshner, and R. Watkins, Mon. Not. R. Astron. Soc. **420**, 447 (2012), 1111.0631.
  - [46] R. Watkins, T. Allen, C. J. Bradford, A. Ramon, and o. Walker, Mon. Not. R. Astron. Soc. **524**, 1885 (2023), 2302.02028.
  - [47] A. Kashlinsky, F. Atrio-Barandela, H. Ebeling, A. Edge, and D. Kocevski, Astrophys. J. Lett. **712**, L81 (2010), 0910.4958.
  - [48] Y.-Z. Ma, C. Gordon, and H. A. Feldman, Phys. Rev. D **83**, 103002 (2011), 1010.4276.
  - [49] S. G. Biern and J. Yoo, J. Cosmol. Astropart. Phys. **026** (2017), 1704.07380.
  - [50] E. Mitsou, J. Yoo, and M. Magi, arXiv e-prints arXiv:2302.00427 (2023), 2302.00427.

- [51] M. Magi and J. Yoo, Phys. Lett. B **846**, 138204 (2023), 2306.09406.
- [52] S. Weinberg, *Gravitation and Cosmology: Principles and Applications of the General Theory of Relativity* (Wiley-VCH, New York, ISBN 0-471-92567-5, 1972).
- [53] P. J. E. Peebles, *Principles of Physical Cosmology* (Princeton University Press, Princeton, 1993).
- [54] J. Larena, Phys. Rev. D **79**, 084006 (2009), 0902.3159.
- [55] I. A. Brown, J. Latta, and A. Coley, Phys. Rev. D **87**, 043518 (2013), 1211.0802.
- [56] É. É. Flanagan and R. M. Wald, Phys. Rev. D **54**, 6233 (1996), gr-qc/9602052.
- [57] S. R. Green and R. M. Wald, Class. Quant. Grav. **31**, 234003 (2014), 1407.8084.
- [58] J. Adamek, C. Clarkson, R. Durrer, and M. Kunz, Phys. Rev. Lett. **114**, 051302 (2015), 1408.2741.
- [59] M. Gasperini, G. Marozzi, F. Nugier, and G. Veneziano, J. Cosmol. Astropart. Phys. **7**, 008 (2011), 1104.1167.
- [60] J. Yoo, E. Mitsou, N. Grimm, R. Durrer, and A. Refregier, J. Cosmol. Astropart. Phys. **2019**, 015 (2019), 1905.08262.
- [61] E. Mitsou, J. Yoo, R. Durrer, F. Scaccabarrozi, and V. Tansella, Physical Review Research **2**, 033004 (2020), 1905.01293.
- [62] E. K. Conklin, Nature (London) **222**, 971 (1969).
- [63] P. J. E. Peebles, *Physical cosmology* (Princeton University Press, Princeton, 1971).
- [64] M. Kamionkowski and L. Knox, Phys. Rev. D **67**, 063001 (2003), astro-ph/0210165.
- [65] A. Challinor and F. van Leeuwen, Phys. Rev. D **65**, 103001 (2002), astro-ph/0112457.
- [66] D. Jeong, J. Chluba, L. Dai, M. Kamionkowski, and X. Wang, Phys. Rev. D **89**, 023003 (2014), 1309.2285.
- [67] R. K. Sachs and A. M. Wolfe, Astrophys. J. **147**, 73+ (1967).
- [68] S. Baumgartner and J. Yoo, Phys. Rev. D **103**, 063516 (2021), 2012.03968.
- [69] U. Seljak, Astrophys. J. Lett. **435**, L87 (1994).
- [70] W. Hu and N. Sugiyama, Astrophys. J. **444**, 489 (1995), astro-ph/9407093.
- [71] J. P. Zibin and D. Scott, Phys. Rev. D **78**, 123529 (2008), 0808.2047.
- [72] G. F. R. Ellis and R. Durrer, arXiv e-prints arXiv:1806.09530 (2018), 1806.09530.
- [73] E. Mitsou and J. Yoo, Springer Briefs in Physics arXiv:1908.10757 (2020), 1908.10757.
- [74] A. G. Riess, A. V. Filippenko, P. Challis, A. Clocchiatti, A. Diercks, P. M. Garnavich, R. L. Gilliland, C. J. Hogan, S. Jha, R. P. Kirshner, et al., Astron. J. **116**, 1009 (1998), arXiv:astro-ph/9805201.
- [75] S. Perlmutter, G. Aldering, G. Goldhaber, R. A. Knop, P. Nugent, P. G. Castro, S. Deustua, S. Fabbro, A. Goobar, D. E. Groom, et al., Astrophys. J. **517**, 565 (1999), arXiv:astro-ph/9812133.
- [76] J. Colin, R. Mohayaee, S. Sarkar, and A. Shafieloo, Mon. Not. R. Astron. Soc. **414**, 264 (2011), 1011.6292.
- [77] A. Sah, M. Rameez, S. Sarkar, and C. G. Tsagas, European Physical Journal C **85**, 596 (2025), 2411.10838.
- [78] A. G. Riess, W. Yuan, L. M. Macri, D. Scolnic, D. Brout, S. Casertano, D. O. Jones, Y. Murakami, G. S. Anand, L. Breuval, et al., Astrophys. J. Lett. **934**, L7 (2022), 2112.04510.
- [79] D. Scolnic, D. Brout, A. Carr, A. G. Riess, T. M. Davis, A. Dwomoh, D. O. Jones, N. Ali, P. Charvu, R. Chen, et al., Astrophys. J. **938**, 113 (2022), 2112.03863.
- [80] D. Brout, D. Scolnic, B. Popovic, A. G. Riess, A. Carr, J. Zuntz, R. Kessler, T. M. Davis, S. Hinton, D. Jones, et al., Astrophys. J. **938**, 110 (2022), 2202.04077.
- [81] A. G. Riess, W. H. Press, and R. P. Kirshner, Astrophys. J. Lett. **445**, L91 (1995), astro-ph/9412017.
- [82] J. Colin, R. Mohayaee, M. Rameez, and S. Sarkar, Astron. Astrophys. **631**, L13 (2019), 1808.04597.
- [83] F. Sorrenti, R. Durrer, and M. Kunz, J. Cosmol. Astropart. Phys. **2023**, 054 (2023), 2212.10328.
- [84] F. Sorrenti, R. Durrer, and M. Kunz, arXiv e-prints arXiv:2403.17741 (2024), 2403.17741.
- [85] F. Sorrenti, R. Durrer, and M. Kunz, J. Cosmol. Astropart. Phys. **2024**, 003 (2024), 2407.07002.
- [86] C. A. P. Bengaly, J. S. Alcaniz, and C. Pigozzo, Phys. Rev. D **109**, 123533 (2024), 2402.17741.
- [87] M. Sasaki, Mon. Not. R. Astron. Soc. **228**, 653 (1987).
- [88] C. Bonvin, R. Durrer, and M. A. Gasparini, Phys. Rev. D **73**, 023523 (2006), arXiv:0511183.
- [89] L. Hui and P. B. Greene, Phys. Rev. D **73**, 123526 (2006), astro-ph/0512159.
- [90] C. Clarkson, G. F. R. Ellis, A. Faltenbacher, R. Maartens, O. Umeh, and J.-P. Uzan, Mon. Not. R. Astron. Soc. **426**, 1121 (2012), 1109.2484.
- [91] P. Fleury, H. Dupuy, and J.-P. Uzan, Phys. Rev. D **87**, 123526 (2013), 1302.5308.
- [92] I. Ben-Dayan, R. Durrer, G. Marozzi, and D. J. Schwarz, Phys. Rev. Lett. **112**, 221301 (2014), 1401.7973.
- [93] N. Kaiser and M. J. Hudson, Mon. Not. R. Astron. Soc. **450**, 883 (2015), 1411.6339.
- [94] J. Yoo, Class. Quant. Grav. **31**, 234001 (2014), arXiv:1409.3223.
- [95] J. Yoo and F. Scaccabarrozi, J. Cosmol. Astropart. Phys. **9**, 046 (2016), 1606.08453.
- [96] J. Yoo, N. Grimm, E. Mitsou, A. Amara, and A. Refregier, J. Cosmol. Astropart. Phys. **4**, 029 (2018), 1802.03403.
- [97] F. Scaccabarrozi and J. Yoo, J. Cosmol. Astropart. Phys. **6**, 007 (2017), 1703.08552.
- [98] D. Brout, D. Scolnic, B. Popovic, A. G. Riess, A. Carr, and o. Zuntz, Astrophys. J. **938**, 110 (2022), 2202.04077.
- [99] J. Yoo, Phys. Rev. D **101**, 043507 (2020), 1911.07869.
- [100] C. W. Stubbs, D. Sweeney, J. A. Tyson, and LSST Collaboration, in *American Astronomical Society Meeting Abstracts* (2004), vol. 36 of *Bulletin of the American Astronomical Society*, p. 108.02.
- [101] S. G. Biern and J. Yoo, J. Cosmol. Astropart. Phys. **4**, 045 (2017), 1606.01910.
- [102] G. Domènech, R. Mohayaee, S. P. Patil, and S. Sarkar, J. Cosmol. Astropart. Phys. **2022**, 019 (2022), 2207.01569.
- [103] G. Kashyap, N. K. Singh, and P. Jain, arXiv e-prints arXiv:2504.14190 (2025), 2504.14190.
- [104] M. F. Skrutskie, R. M. Cutri, R. Stiening, M. D. Weinberg, S. Schneider, J. M. Carpenter, C. Beichman, R. Capps, T. Chester, J. Elias, et al., Astron. J. **131**, 1163 (2006).
- [105] H. T. Intema, P. Jagannathan, K. P. Mooley, and D. A. Frail, Astron. Astrophys. **598**, A78 (2017), 1603.04368.
- [106] P. da Silveira Ferreira and V. Marra, J. Cosmol. Astropart. Phys. **2024**, 077 (2024), 2403.14580.
- [107] J. Yoo, Phys. Rev. D **79**, 023517 (2009), arXiv:0808.3138.
- [108] J. Yoo, J. Cosmol. Astropart. Phys. **2023**, 054 (2023), 2212.03573.
- [109] J. Yoo, A. L. Fitzpatrick, and M. Zaldarriaga, Phys. Rev. D **80**, 083514 (2009), arXiv:0907.0707.
- [110] J. Yoo, Phys. Rev. D **82**, 083508 (2010), arXiv:1009.3021.
- [111] A. Challinor and A. Lewis, Phys. Rev. D **84**, 043516 (2011), arXiv:1105.5292.

- [112] C. Bonvin and R. Durrer, *Phys. Rev. D* **84**, 063505 (2011), arXiv:1105.5280.
- [113] D. Jeong, F. Schmidt, and C. M. Hirata, *Phys. Rev. D* **85**, 023504 (2012), arXiv:1107.5427.
- [114] R. Narayan, *Astrophys. J. Lett.* **339**, L53 (1989).
- [115] M. Bartelmann, *Astron. Astrophys.* **298**, 661 (1995), arXiv:astro-ph/9407091.
- [116] B. Jain, R. Scranton, and R. K. Sheth, *Mon. Not. R. Astron. Soc.* **345**, 62 (2003), arXiv:astro-ph/0304203.
- [117] R. Scranton et al., *Astrophys. J.* **633**, 589 (2005), arXiv:astro-ph/0504510.
- [118] F. Scaccabarrozi, J. Yoo, and S. G. Biern, *J. Cosmol. Astropart. Phys.* **10**, 024 (2018), 1807.09796.
- [119] N. Grimm, F. Scaccabarrozi, J. Yoo, S. G. Biern, and J.-O. Gong, *J. Cosmol. Astropart. Phys.* **2020**, 064 (2020), 2005.06484.
- [120] T. Nadolny, R. Durrer, M. Kunz, and H. Padmanabhan, *J. Cosmol. Astropart. Phys.* **2021**, 009 (2021), 2106.05284.
- [121] C. Dalang and C. Bonvin, *Mon. Not. R. Astron. Soc.* **512**, 3895 (2022), 2111.03616.
- [122] C. Guandalin, J. Piat, C. Clarkson, and R. Maartens, *Astrophys. J.* **953**, 144 (2023).
- [123] S. von Hausegger, *Mon. Not. R. Astron. Soc.* **535**, L49 (2024), 2404.07929.
- [124] J. N. Fry, *Astrophys. J. Lett.* **461**, L65+ (1996).
- [125] M. Yoon and D. Huterer, *Astrophys. J. Lett.* **813**, L18 (2015), 1509.05374.
- [126] A. Nusser and P. Tiwari, *Astrophys. J.* **812**, 85 (2015), 1505.06817.
- [127] J. Yoo and J.-O. Gong, *J. Cosmol. Astropart. Phys.* **7**, 017 (2016), 1602.06300.
- [128] P. R. M. Eisenhardt, F. Marocco, J. W. Fowler, A. M. Meisner, J. D. Kirkpatrick, N. Garcia, T. H. Jarrett, R. Koontz, E. J. Marchese, S. A. Stanford, et al., *Astrophys. J. Suppl. Ser.* **247**, 69 (2020), 1908.08902.
- [129] R. E. Smith, J. A. Peacock, A. Jenkins, S. D. M. White, C. S. Frenk, F. R. Pearce, P. A. Thomas, G. Efstathiou, and H. M. P. Couchman, *Mon. Not. R. Astron. Soc.* **341**, 1311 (2003), arXiv:astro-ph/0207664.
- [130] J. Chen, P. Zhang, Y. Zheng, Y. Yu, and Y. Jing, *Astrophys. J.* **861**, 58 (2018), 1803.00728.
- [131] W. H. Press and P. Schechter, *Astrophys. J.* **187**, 425 (1974).
- [132] J. Yoo and D. Eisenstein, *Astrophys. J. Lett.* **979**, L35 (2025), 2410.00951.